PROCEEDINGS OF THE ROYAL SOCIETY A MATHEMATICAL, PHYSICAL & ENGINEERING SCIENCES

On the theory of advective effects on biological dynamics in the sea

Allan R. Robinson

Proc. R. Soc. Lond. A 1997 **453**, 2295-2324
doi: 10.1098/rspa.1997.0123

On the theory of advective effects on biological dynamics in the sea

By Allan R. Robinson

Division of Engineering and Applied Sciences, Department of Earth and Planetary Sciences, Harvard University, Cambridge, MA 01238, USA

A general theoretical approach to the study of advective effects on biological oceanographic dynamics is formulated and some simple examples are presented. The theory of characteristics provides a model which rigorously combines aspects of local biological dynamics with consideration of fluid particle flow along Lagrangian trajectories. A local kinematical analysis is carried out for gradients both of velocity and of biological state variables. This is followed by a study of the effects of a stretching deformation, which contains a frontogenetic effect, on one- to three-component biological systems. Problems include the approach to local biological equilibria and the stabilities of the equilibrium states; the competition between biological and advective equilibria; and nonlinear grazing processes and nutrient utilization.

1. Introduction

Biological dynamics in the sea involves interactions among physical, biological and chemical processes and coupled processes. A multitude of scales and phenomena are involved, many of which are as yet unknown. Research in interdisciplinary theory and modelling is accelerating, and relevant studies range from idealized isolated process studies to attempts at simulating complex and realistic oceanic dynamics. Concomitantly biological dynamical studies are carried out in zero, one, two and three spatial dimensions. One aspect of the interpretation of some zero-dimensional studies involves the concept of local biological dynamics and equilibria. In such cases the physics may be assumed to be unimportant or may be parametrized by scale-separation hypotheses.

Physical processes which influence the biology consist of physiological effects such as temperature-dependent processes, diffusion and mixing and advection. Physical processes may compete with or enhance biological processes. Advective effects, which are perhaps least well understood theoretically, are isolated as the focus of the present study. Advection involves the movement of biological material via the physical flow field. Vertical and horizontal velocities transport and entrap dissolved and particulate matter over multiple scales in space and time. A large variety of relevant phenomenological flow structures occur in the ocean, and their associated advective effects may be best treated deterministically or statistically.

The present study adopts an idealized general theoretical approach to the study of advective effects. The attempt is to identify and expose some basic processes which may aid in the interpretation of simulations and which may form the basis of further more realistic studies. The focus is primarily upon the influence of a

Proc. R. Soc. Lond. A (1997) **453**, 2295–2324
Printed in Great Britain

TEX Paper

deformation gradient in the flow field on a dynamically active tracer field, and the results may have some general applications to, for example, chemical and engineering dynamics. The general model, which can be related to zero-dimensional biological dynamics and fluid particle trajectories, is introduced in § 2. Sections 3, 4 and 5 subsequently deal, respectively, with advective, biological and interactive processes. Section 6 summarizes and concludes.

2. The model

(a) *Formulation*

Consider an n-component biological system with the state variables

$$\phi_i(x, y, z, t), \quad i = 1, \ldots, n, \tag{2.1}$$

for the mass densities of plankton, nutrients, etc., in suitable units of mass (m) divided by volume (ℓ^3). The state variables are assumed to be continuous fields (Batchelor 1967, ch. 1), diffusion is neglected, and the necessity of Reynolds-averaging of physical and biological turbulent fluctuations in the fluid (Hinze 1975; Okubo 1980, ch. 10) is ignored. If, in the absence of motion, the biology is governed by the zero (spatial) dimensional dynamics

$$\begin{aligned} \frac{\mathrm{d}\phi_i}{\mathrm{d}t} &= B_i(\phi_1, \ldots, \phi_n), \quad i = 1, \ldots, n, \\ &\equiv B_i(\phi_j), \quad j = 1, \ldots, n, \end{aligned} \tag{2.2}$$

then the dynamics, in the presence of a flow field, is governed by

$$\frac{\mathrm{D}\,\phi_i}{\mathrm{D}\,t} = B(\phi_j). \tag{2.3}$$

Note that the argument ϕ_j of B symbolically represents the arbitrary individual dependencies of B upon $\phi_1 \cdots \phi_n$.

The advective derivative in Cartesian coordinates is

$$\frac{\mathrm{D}\,\phi_i}{\mathrm{D}\,t} = \frac{\partial\phi_i}{\partial t} + u\frac{\partial\phi_i}{\partial x} + v\frac{\partial\phi_i}{\partial y} + w\frac{\partial\phi_i}{\partial z} \tag{2.4a}$$

$$= \frac{\partial\phi_i}{\partial t} + \frac{\partial}{\partial x}(u\phi_i) + \frac{\partial}{\partial y}(v\phi_i) + \frac{\partial}{\partial z}(w\phi_i), \tag{2.4b}$$

where the equivalence of the two forms of equation (2.4) arises from the conservation of mass, or continuity equation, of an incompressible liquid

$$\frac{\partial u}{\partial x} + \frac{\partial v}{\partial y} + \frac{\partial w}{\partial z} = 0. \tag{2.5}$$

In most cases of interest we will represent biological activity by simple self-interactions and predator–prey interactions (Murray 1993, ch. 3), with

$$B_i(\phi_j) = \phi_i\left(a_{i0} + \sum_{j=1}^{n} a_{ij}\phi_j\right). \tag{2.6}$$

The advective derivative $\mathrm{D}/\mathrm{D}\,t$, as given by equation (2.4*a*), represents the time rate of change of ϕ_i following the fluid motion, but expressed in the Eulerian viewpoint for a space–time field (equation (2.1)) at a fixed point in the flow (Lamb 1932,

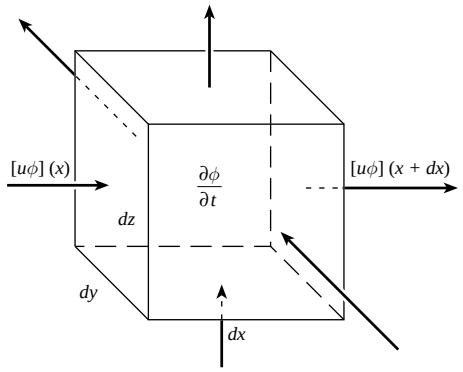

Figure 1. At the fixed point (x, y, z) the net difference of rate of inflow and outflow of ϕ through the six faces tends to change the amount of ϕ within the infinitesimal volume.

ch. 1; Batchelor 1967, ch. 2). From the Lagrangian viewpoint, i.e. following tagged fluid particles along finite trajectories, zero-dimensional biological dynamics is simply occurring within each particle. Equation (2.4 *b*) presents an alternative useful interpretation of the advective process at a fixed Eulerian point from a flux viewpoint. Taking into account all processes which act as effective sources (or sinks), equations (2.2) and (2.3) are simply point-wise statements of the conservation of ϕ_i. The local advective flux (units of mass per unit area per unit time $-m\ell^{-2}t^{-1}$) is

$$\mathcal{F}_{\mathrm{A}} = u\phi_i\hat{\boldsymbol{i}} + +v\phi_i\hat{\boldsymbol{j}} + w\phi_i\hat{\boldsymbol{k}}, \tag{2.7}$$

and its divergence (convergence) $\nabla\cdot\mathcal{F}_{\mathrm{A}}$ can provide a local sink (source) of biomass. The flux divergence process is illustrated for an infinitesimal Cartesian volume in figure 1. However, recall that the divergence theorem in general relates the net normal flux through the surface S of an arbitrary volume V to the volume integral of the divergence, and that for an infinitesimal volume

$$\nabla\cdot\mathcal{F} = \lim_{V\to 0}\frac{1}{V}\int_S \hat{\boldsymbol{n}}\cdot\mathcal{F}\,\mathrm{d}S, \tag{2.8}$$

is the mass outflow per unit volume per unit time.

In the present study we will restrict ourselves to two- (spatial) dimensional flows, whence continuity implies the existence of a stream function $\psi(x, y, t)$ such that

$$u(x, y, t) = -\frac{\partial\psi}{\partial y}, \quad v(x, y, t) = \frac{\partial\psi}{\partial x}, \tag{2.9}$$

satisfy equation (2.5) identically. The x–y plane can be regarded as a horizontal surface or a vertical section in the ocean. In the former case, if the flow is of large enough scale to be in geostrophic balance (Pond & Pickard 1978), the stream function is related to the geostrophic pressure (p) via $p = \rho_0 f\psi$, where ρ_0 is the mean density and $f = 2\Omega\sin\theta$ is the Coriolis parameter (Ω is the Earth's rotation and θ is the latitude).

It will be convenient to express the model in both dimensional (2.10 *a*) and non-dimensional (2.10 *b*) forms. For the latter case: the ϕ_i will all be scaled by a representative mass density M; time by t_0; distance by L; and speed by u_0. Since the context will be clear, we will use identical symbols for both the dimensional and non-dimensional versions for the dependent and independent variables. Thus the

final model takes the forms

$$\frac{\partial \phi_i}{\partial t} + u\frac{\partial \phi_i}{\partial x} + v\frac{\partial \phi_i}{\partial y} = B_i(\phi_j) = \phi_i\left(a_{io} + \sum_{j=1}^{n} a_{ij}\phi_j\right) \tag{2.10 a}$$

$$\frac{\partial \phi_i}{\partial t} + \alpha\left[u\frac{\partial \phi_i}{\partial x} + v\frac{\partial \phi_i}{\partial y}\right] = B_i(\phi_j) = \phi_i\left[\alpha_{io} + \sum_{j=1}^{n} \alpha_{ij}\phi_j\right]. \tag{2.10 b}$$

In equation (2.10 *b*), the non-dimensional parameters

$$\alpha \equiv \frac{u_0 t_0}{L}, \quad \alpha_{io} \equiv t_0 a_{io}, \quad \alpha_{ij} \equiv M t_0 a_{ij}, \tag{2.10 c}$$

characterize the relative importance of local time changes ($\partial\phi/\partial t$) due, respectively, to advection, net birth or death, self-interaction (α_{ii}) and predator–prey interactions (grazing).

The left-hand side alone represents local time change plus the advection of the scalar field and the right-hand side alone, the 'zero-dimensional' local biological dynamics. In general, scalar fields are characterized as *passive* or *active* depending upon whether or not they influence the flow field, and *inert* or *dynamical* depending upon whether they are simply advected or have sources and sinks due, for example, to radioactivity, chemical reactions or biological activity.

A version of the parameter α (denoted S) based upon the growth rate $t_0 = a_{i0}^{-1}$ was first identified by Obrien & Wroblewski (1973) as an appropriate measure of advective effects. Platt & Denman (1975) and Platt *et al.* (1977) scaled a general biomass equation and estimated ranges of relative ratios from data available at that time, which are generally still relevant. A useful quantitative overview of the non-dimensional approach is also presented by Wroblewski (1983). A recent example of a non-dimensional analysis of scale-dependent physical and biological processes governing the distribution and variability of biomass for a particular species is provided by Horne & Schneider (1994).

(*b*) *Solution*

Equations (2.10) are a set of n-coupled first-order partial differential equations. Since the left-hand sides are linear in the ϕ_i, and there are identical operators on each of the ϕ_i, it is a quasi-linear set with the same principal parts which can be solved symbolically via the method of characteristics (Courant & Hilbert 1989, ch. II, Appendix I). Consider a solution given in terms of a parametric variable s in the form

$$\phi_i(x(s), y(s), t(s)). \tag{2.11 a}$$

Then if

$$\frac{\mathrm{d}\phi_i}{\mathrm{d}s} = \frac{\partial \phi_i}{\partial x}\frac{\mathrm{d}x}{\mathrm{d}s} + \frac{\partial \phi_i}{\partial y}\frac{\mathrm{d}y}{\mathrm{d}s} + \frac{\partial \phi_i}{\partial t}\frac{\mathrm{d}t}{\mathrm{d}s} \tag{2.11 b}$$

and if

$$\frac{\mathrm{d}t}{\mathrm{d}s} = 1, \quad \frac{\mathrm{d}x}{\mathrm{d}s} = u(x, y, t), \quad \frac{\mathrm{d}y}{\mathrm{d}s} = v(x, y, t) \tag{2.12 a}$$

and also

$$\frac{\mathrm{d}\phi_i}{\mathrm{d}s} = B_i(\phi_1 \cdots \phi_n), \tag{2.12 b}$$

then equation (2.11) solves equation (2.10). The solutions to (2.12) are called the family of characteristic curves belonging to equations (2.10).

The parametric initial value problem specifies data, without loss of generality, at $s = 0$. The initial values of all the variables are to be specified in terms of two additional parametric variables (r, q), since there are three independent variables in each of equations (2.10 *a*), (2.10 *b*). We designate

$$t(s = 0; r, q) = a(r, q), \quad x(0, r, q) = b(r, q), \quad y(0, r, q) = c(r, q) \tag{2.13 a}$$

and

$$\phi_i(0, r, q) = d_i(r, q). \tag{2.13 b}$$

The formal procedure is to solve (2.12 *a*) subject to conditions (2.13 *a*) to yield

$$t(s, r, q), \quad x(s, r, q), \quad y(s, r, q) \tag{2.14 a}$$

and then to invert to obtain

$$s(x, y, t), \quad r(x, y, t), \quad q(x, y, t). \tag{2.14 b}$$

The set of equations (2.12 *b*) is solved subject to conditions (2.13 *b*) to yield

$$\phi_i(s, r, q), \tag{2.15 a}$$

which upon insertion of the parametric variables (2.14 *b*) provides the biological fields in physical space

$$\phi_i(x, y, t). \tag{2.15 b}$$

The structure of the formal solution of the preceding paragraph is dynamically interesting and provides a valuable framework for interpreting coupled biological and physical processes. Advective processes appear in (2.12 *a*) directly in terms of the Lagrangian trajectory equations but in the s-domain. Similarly, the zero-dimensional biological dynamics appear in the s-domain in equation (2.12 *b*). A special but important class of problems involves the specification of initial fields in the time domain, i.e. at $t = 0$. The first of (2.12 *a*) is always directly integrable to $t = s + a(r, q)$ and for this special case we have $a = 0$, $s = t$. Now (2.12 *b*) is the local biological dynamics, but the local 'biological equilibrium' (2.15 *a*) can be altered significantly by the advective effects through r, q as given by (2.14 *b*).

To illustrate the solution procedure, we consider the simplest example of the exponential (Malthusian) growth of phytoplankton (ϕ_i) with unlimited light and nutrient in the presence of a spatially uniform and constant velocity field (u_0, v_o). We seek the time evolution of an initial spatial distribution of ϕ. Equations (2.12 *a*), (2.12 *b*) with reference to (2.10 *a*) become

$$\frac{\mathrm{d}t}{\mathrm{d}s} = 1, \quad \frac{\mathrm{d}x}{\mathrm{d}s} = u_0, \quad \frac{\mathrm{d}y}{\mathrm{d}s} = v_0, \quad \frac{\mathrm{d}\phi_1}{\mathrm{d}s} = a_{10}\phi_1, \tag{2.16 a}$$

with solutions (2.14 *a*), (2.15 *a*)

$$t = s + a, \quad x = u_0 s + b, \quad y = u_0 s + c, \quad \phi_1 = d_1 \mathrm{e}^{a_{10} s}. \tag{2.16 b}$$

The time domain initial condition,

$$\phi_1(x, y, t = 0) = d(x, y), \tag{2.16 c}$$

requires for solution to equations (2.13)

$$a = 0, \quad b = r, \quad c = q, \tag{2.16 d}$$

whence (2.14 *b*) becomes simply

$$s = t, \quad r = x - u_0 t, \quad q = y - v_0 t. \tag{2.16 e}$$

The final solution (2.15 *b*)

$$\phi_1 = d_1(x - u_0 t, y - v_0 t)\mathrm{e}^{a_{10} t}, \tag{2.16 f}$$

is an advective translation of the initial pattern with the plankton growing uniformly everywhere. The simple structure of (2.16 *f*) as a product of advective effects times biological effects is generally deceptive as will be seen in § 5.

An alternative formulation of the model in terms of the stream function defined in equation (3.2) can be useful. We consider a time-independent stream function $\psi(x, y)$ as an independent variable and seek $\phi_i(\psi, y, t)$. Since

$$\left.\frac{\partial \phi}{\partial x}\right|_{y,t} = \left.\frac{\partial \phi}{\partial \psi}\right|_{y,t} \cdot \left.\frac{\partial \psi}{\partial x}\right|_{y}, \quad \left.\frac{\partial \phi}{\partial y}\right|_{x,t} = \left.\frac{\partial \phi}{\partial \psi}\right|_{y,t} \cdot \left.\frac{\partial \psi}{\partial y}\right|_{x} + \left.\frac{\partial \phi}{\partial y}\right|_{\psi,t}, \tag{2.17 a}$$

equation (2.10 *a*) becomes with (ψ, y) as independent variables

$$\frac{\partial \phi_i}{\partial t} + v(\psi, y)\frac{\partial \phi_i}{\partial y} = B_i(\phi_j). \tag{2.17 b}$$

Equation (2.17 *b*) contains the familiar result that a time-independent distribution of a passive inert scalar can be any functional $F(\psi)$ of the stream function field. More generally, if a passive dynamic scalar is distributed on the streamlines of the flow, it will evolve everywhere according to zero-dimensional dynamics, i.e. (2.17 *b*) with $(\partial \phi_i/\partial y)|_{\psi,t} = 0$ reduces to equation (2.2). The alternative to equation (2.12) becomes

$$\frac{\mathrm{d}t}{\mathrm{d}s} = 1, \quad \frac{\mathrm{d}y}{\mathrm{d}s} = v(\psi, y), \quad \frac{\mathrm{d}\phi_i}{\mathrm{d}s} = B_i. \tag{2.17 c}$$

Since (2.17 *b*) now has only two explicit independent variables, only one additional parameter (r) is needed for the solution to (2.17 *c*); ψ is a parameter of the solution. However, initial x-dependence must be represented as $x(\psi, y)$.

3. Advective processes

In this section we consider solutions to equations (2.10), (2.12) with $B_i = 0$ and (u, v) specified, i.e. the advection of a passive inert scalar. Even under these simplifications, analytical solutions for the trajectories are difficult and the flow of a tracer patch can be quite complex due to the stretching and folding of an initial distribution. Even smooth flows can give rise to chaotic advection (Ottino 1989, 1990). Interesting examples of the complex trajectories that occur in oceanic mesoscale waves and coherent vortices are presented by Flierl (1981) and Dewar & Flierl (1985).

(*a*) *Local analysis*

Consider the initial value problem in the time domain. To provide some general insight we expand both an initial scalar tracer field and the advecting velocity in Taylor series in the neighbourhood of the point $(0, 0)$. Since the tracer fields are inert and uncoupled we drop the subscript i. Thus

$$\phi(x, y, 0) = c_0 + c_1 x + c_2 y, \tag{3.1 a}$$

$$u = u_0 + u_1 x + u_2 y, \tag{3.1 b}$$

$$v = v_0 + v_1 x + v_2 y.$$

If the flow is non-divergent, then $v_2 = -u_1$ and a stream function exists. The case of pure translation is given by equation (2.16 *f*) with $a_{10} = 0$. Removing the translation, the solution equations (2.14)–(2.15) to equations (2.11)–(2.12) are given by

$$\phi = c_0 + c_1 r + c_2 q, \tag{3.1 c}$$

$$s = t,$$

$$r = \left[\cosh\gamma t - \frac{u_1}{\gamma}\sinh\gamma t\right] x - \left[\frac{u_2}{\gamma}\sinh\gamma t\right] y, \tag{3.1 d}$$

$$q = -\left[\frac{v_1}{\gamma}\sinh\gamma t\right] x + \left[\cosh\gamma t + \frac{u_1}{\gamma}\sinh\gamma t\right] y,$$

where

$$\gamma \equiv [u_1^2 + u_2 v_1]^{1/2}.$$

Note that at $t = 0$, $r = x$, $q = y$. Asymptotically for real γ as $t \to \infty$,

$$r = \tfrac{1}{2}\mathrm{e}^{\gamma t}\left[\left(1 - \frac{u_1}{\gamma}\right) x - \frac{u_2}{\gamma} y\right], \tag{3.1 e}$$

$$q = \tfrac{1}{2}\mathrm{e}^{\gamma t}\left[-\frac{v_1 x}{\gamma} + \left(1 + \frac{u_1}{\gamma}\right) y\right].$$

Thus a mechanism for the intensification with time of the initial tracer gradient is inherent in the shear of the flow field. However, the general solution (3.1) is quite complicated, and γ may be real or imaginary.

Insight into basic advective processes can be gained by a decomposition of the velocity gradient into its fundamental kinematic parts: divergence (ξ), stretching deformation (ν), vorticity (ω), shearing deformation (μ)

$$\left.\begin{aligned} \xi &= u_x + v_y = u_1 + v_2 = 0, \\ \nu &= u_x - v_y = u_1 - v_2 = 2u_1, \\ \omega &= v_x - u_y = v_1 - u_2, \\ \mu &= v_x + u_y = v_1 + v_2 = v_1 - u_1, \end{aligned}\right\} \tag{3.2}$$

as is traditional in fluid dynamics (Batchelor 1967), meteorology (Stewart 1945) and oceanography (Kirwan *et al.* 1994). The pure effects of each type of motion are shown on figure 2. The divergence and vorticity are invariant with respect to coordinate frame rotations, but not the deformations. However, a rotation through an appropriate angle into the principal axes of deformation will zero the shearing deformation. Thus here we need be concerned only with the effects of vorticity and stretching deformation.

To illustrate the effects of vorticity we set $u_1 = 0$ and $u_2 = -v_1$, whence $\omega = 2v_1$. Then γ is imaginary and

$$r = x\cos v_1 t + y\sin v_1 t, \quad q = -x\sin v_1 t + y\cos v_1 t. \tag{3.3}$$

Inserting (3.3) into (3.1 *c*) shows that the tracer gradients are simply rotated in space with period (π/ω).

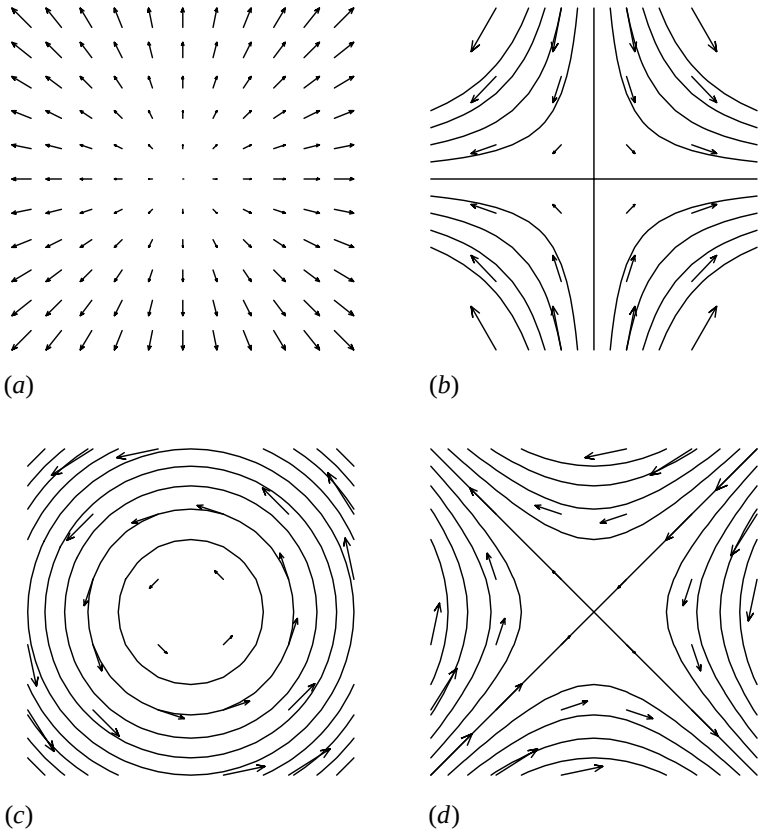

Figure 2. Fundamental kinematic components of a velocity gradient: (*a*) divergence; (*b*) stretching deformation; (*c*) vorticity; (*d*) shearing deformation.

To illustrate the effects of deformation we set $v_1 = u_2 = 0$; and the solution is now

$$r = x\mathrm{e}^{-u_1 t}, \quad q = y\mathrm{e}^{u_1 t}, \tag{3.4\,a}$$

$$\phi = c_0 + c_1 x\mathrm{e}^{-u_1 t} + c_2 y\mathrm{e}^{u_1 t}. \tag{3.4\,b}$$

Referring to figure 2*b*, it can be seen that the hyperbolic flow $\psi = -u_1 xy$ is towards the x-axis (axis of contraction) and away from the y-axis (axis of dilation). The effect is to increase initial y-gradients of the tracer and to decrease initial x-gradients. As the flow continues in time, the gradient intensifies without limit.

(*b*) *Frontogenesis*

The role of deformation fields as a 'trigger' mechanism for the generation of physical fronts in the atmosphere, or the signal that frontogenesis is occurring has been known for some time (Bergeron 1928; Petterson 1935). The analogous mechanism is known to act as a causal mechanism for frontogenesis in the oceans (Simpson & James 1986). Oceanic fronts have been identified as locations of intensified biological activity because of frontal upwelling of nutrients. It should also be recognized that the processes that cause strong physical gradients of, for example, temperature, will also tend directly to concentrate and cause strong gradients of biological and chemical tracers, i.e. to generate biological fronts. Convergence (regions of negative ξ) is also a frontogenetic kinematic mechanism, but the thin aspect ratios of the atmosphere

and ocean (depth much less than horizontal scales) render them almost horizontally non-divergent and the process is less important.

Saucier (1953) describes a classical meteorological method for analysing the tendency for frontogenesis from the horizontal deformation of wind fields. The angle (θ) required for rotation of the axes into principal axes, and the resultant principal stretching deformation (ν_{p}) are given by

$$\theta = \tfrac{1}{2}\tan^{-1}[(v_1 + u_2)/(u_1 - v_2)], \tag{3.5}$$

$$\nu_{\mathrm{p}} = [(u_1 - v_2)^2 + (v_1 + u_2)^2]^{1/2}.$$

He also presents a method for streamline analysis of deformation and a method for evaluating deformation under the geostrophic approximation. The existence of a deformation field is a sufficient condition for frontogenesis, and dynamical studies have been carried out for the atmospheric fronts whose development is ultimately limited by secondary circulation (Stone 1966) and dissipative processes using various approximate dynamical models. To discuss the rate of change of ϕ moving with the fluid, use is made of the so-called frontogenesis function $\mathrm{D}/\mathrm{D}\,t|\nabla\phi|^2$ (Hoskins 1982). In certain cases, a simple shear normal to the flow direction has been implicated as a generation mechanism (Williams 1967).

(*c*) *Oceanic gradients*

Relatively intense gradients occur in the deep and coastal oceans associated with a variety of scales of motion, phenomena and internal and external driving mechanisms. Permanent fronts separate water masses and give rise to intense boundary and free jets. Permanent convergence zones exist in the equatorial, subtropical and polar oceans. Water-mass-driven, wind-driven and tidally driven fronts occur at and across shelf breaks, in the coastal ocean and in the vicinity of banks. Internal dynamical processes (e.g. instabilities, nonlinear and topographic interactions) populate the ocean with frontal ring vortices, eddies and lenses over a range of meso- and submesoscales. Such fronts and eddies must be expected to produce biological fronts and interactions and to influence biological dynamics. Biological and physical interactions for some types of fronts, have been and are being studied, such as: eastern boundary upwelling systems (Barber & Smith 1981), cold and warm core Gulf Stream rings (The Ring Group 1981; Olson & Backus 1985; Franks *et al.* 1986); tidal fronts (Lynch *et al.* 1995); and eddy–eddy interactions (McGillicuddy *et al.* 1995). Others have only recently been discovered or understood and await interdisciplinary research.

A theoretical study (Kirwan *et al.* 1994) of aspects of nonlinear ocean dynamics is based in part on the local kinematics of horizontal divergence (ξ), deformation (ν) and vorticity (ω). Waves, eddies and submesoscale lenses are considered under various dynamical assumptions. Further and broader studies based in the kinematic approach can be useful to the theory of advective effects in biological dynamics. A number of relevant field studies have been carried out attempting to measure directly the kinematic quantities from the dispersion of float clusters. Inference of ξ, ν and ω is quantitatively difficult and usually sensitive (Kirwan *et al.* 1988, 1992). A recent study (Sanderson 1995) was carried out on the Western Bank of the Scotian Shelf in which the drifters were part of a measurement and modelling system to track cod larvae (Bowen *et al.* 1995). The estimates, considered sensitive, were

$$\omega = (-1.9 \pm 0.06) \times 10^{-5}\ \mathrm{s}^{-1}, \quad \xi = (-9.5 \pm 7) \times 10^{-7}\ \mathrm{s}^{-1},$$

$$\nu = (9.0 \pm 7) \times 10^{-7}\ \mathrm{s}^{-1}, \quad \mu = (1.7 \pm 0.6) \times 10^{-6}\ \mathrm{s}^{-1}.$$

Recall that $(1.16) \times 10^{-5}\,\mathrm{s}^{-1} = (\mathrm{day})^{-1}$. Thus such physical time scales are in the range of some important biological time scales (Denman & Powell 1984; Dickey 1990). Some general scale considerations for effective biological and physical interactions are discussed by Steele (1988), Nihoul & Djendi (1991) and Denman (1992).

4. Biological processes

In this section we summarize some of the dynamical properties of a simple two-component biological system in zero spatial dimensions (see, for example, Freedman 1980; Murray 1993). We assume a predator–prey system with perfect grazing. In the absence of grazing, the prey can achieve an equilibrium value (carrying capacity) but the predator is depleted, e.g. a simple phytoplankton–zooplankton model with unlimited light and nutrient to support photosynthesis.

The relevant equations are (2.2) and (2.6) with non-dimensionalization when desirable as in (2.10) but with $u_0 = 0$. To keep all of the constants in the equations positive, we adopt the notation $\hat{a}_{ij} = -a_{ij}$ if $a_{ij} < 0$, and similarly for α_{ij}. The model equations under the above assumptions are, with $a_{12} = -a_{21}$ and $a_{22} = 0$,

$$\frac{\mathrm{d}\phi_1}{\mathrm{d}t} = \phi_1(a_{10} - \hat{a}_{11}\phi_1 - a_{21}\phi_2), \tag{4.1a}$$

$$\frac{\mathrm{d}\phi_2}{\mathrm{d}t} = \phi_2(-\hat{a}_{20} + a_{21}\phi_1). \tag{4.1b}$$

We shall consider: the linearized stability properties of equilibria; the nonlinear approach to the carrying capacity equilibrium; and nonlinear grazing dynamics. Freedman (1980, ch. 3) reviews properties of this model which he refers to as a Lotka–Volterra system with semidecreasing returns.

Let Φ_i denote a steady-state equilibrium field and introduce the notation

$$\phi_1 = \Phi_1 + \delta, \quad \phi_2 = \Phi_2 + \epsilon, \tag{4.2}$$

with (δ, ϵ) the general differences away from equilibrium. The equilibrium fields satisfy (4.1) with $(\mathrm{d}/\mathrm{d}t) = 0$. Upon addition of (4.1 *a*), (4.1 *b*) and substitution of the result back into (4.1 *a*), there results

$$\Phi_1(a_{10} - \hat{a}_{11}\Phi_1)(\hat{a}_{20} - a_{21}\Phi_1) = 0, \tag{4.3}$$

$$\Phi_2 = \frac{\Phi_1}{\hat{a}_{20}}(a_{10} - \hat{a}_{11}\Phi_1).$$

There are three equilibrium states, namely

$$\Phi_1 = 0, \quad \Phi_2 = 0 \quad (\text{null}), \tag{4.4a}$$

$$\Phi_1 = \frac{a_{10}}{\hat{a}_{11}} \equiv C, \quad \Phi_2 = 0 \quad (\text{carrying capacity}), \tag{4.4b}$$

$$\Phi_1 = \frac{\hat{a}_{20}}{a_{21}} \equiv G, \quad \Phi_2 = G\left(\frac{a_{10}}{\hat{a}_{20}} - \frac{\hat{a}_{11}}{a_{21}}\right) \qquad (\text{grazing}). \tag{4.4c}$$

(*a*) *The null state*

For instability analyses we assume δ, ϵ to be infinitesimal. Then linearization of (4.1 *a*), (4.1 *b*) about the null state (4.4 *a*) decouples the two fields and ϕ_1 is unstable and ϕ_2 is stable. If the ϕ_2 perturbation is suppressed, ϕ_1 will evolve in time to the

carrying capacity equilibrium C. If $\epsilon \neq 0$, ϕ_2 will begin to grow when the second term on the right-hand side of (4.1 *b*) exceeds the first term. Non-dimensionalizing both state variables by $M = C$ and choosing $t_0 = (a_{10})^{-1}$, equations (4.1) become (see (2.10 *c*))

$$\frac{\mathrm{d}\phi_1}{\mathrm{d}t} = \phi_1(1 - \phi_1 - \alpha_{21}\phi_2), \tag{4.5 a}$$

$$\frac{\mathrm{d}\phi_2}{\mathrm{d}t} = \phi_2(-\hat{\alpha}_{20} + \alpha_{21}\phi_1), \tag{4.5 b}$$

where

$$\hat{\alpha}_{20} \equiv \frac{\hat{a}_{20}}{a_{10}}, \quad \alpha_{21} \equiv \frac{a_{21}}{a_{10}}C = \frac{a_{21}}{\hat{a}_{11}}.$$

For a period of time after ϕ_1 begins exponential growth and achieves finite amplitude the departures from equilibrium will be governed by (4.5 *a*) linearized around the null state (4.4 *a*) and the full (4.5 *b*), i.e.

$$\frac{\mathrm{d}\delta}{\mathrm{d}t} - \delta = 0, \tag{4.6 a}$$

$$\frac{\mathrm{d}\epsilon}{\mathrm{d}t} + \epsilon[\hat{\alpha}_{20} - \alpha_{21}\delta] = 0, \tag{4.6 b}$$

with solutions

$$\delta = \delta_0 \mathrm{e}^t, \tag{4.6 c}$$

$$\epsilon = \epsilon_0 \exp[-\hat{\alpha}_{20}t + \alpha_{21}\delta_0\mathrm{e}^t]. \tag{4.6 d}$$

Thus at time t_g determined by

$$t_\mathrm{g} = \ln\left[\frac{\hat{\alpha}_{20}}{\alpha_{21}}\frac{t_\mathrm{g}}{\delta_0}\right], \tag{4.6 e}$$

there will be an explosive growth of the predator ϕ_2.

(*b*) *Carrying capacity*

The carrying capacity equilibrium is governed by equations (4.5) with $\phi_2 \equiv 0$ and $\delta = \phi_1 - 1$. The full δ equation is

$$\frac{\mathrm{d}\delta}{\mathrm{d}t} + \delta(1 + \delta) = 0. \tag{4.7 a}$$

The linearized equation now indicates stability

$$\delta = \delta_0 \mathrm{e}^{-t}, \tag{4.7 b}$$

and the nonlinear approach to equilibrium is given by the logistic growth solution

$$\delta = \frac{\delta_0}{(\delta_0 + 1)\mathrm{e}^t - \delta_0} \tag{4.7 c}$$

$$\phi_1 = \frac{\phi_{10}}{\phi_{10} + (1 - \phi_{10})\mathrm{e}^{-t}}. \tag{4.7 d}$$

Figure 3*a* depicts $\phi_1(t)$; since the mortality is quadratic an excess of ϕ_1 over C is depleted more rapidly than a deficit is enhanced as the carrying capacity equilibrium is approached for all initial conditions.

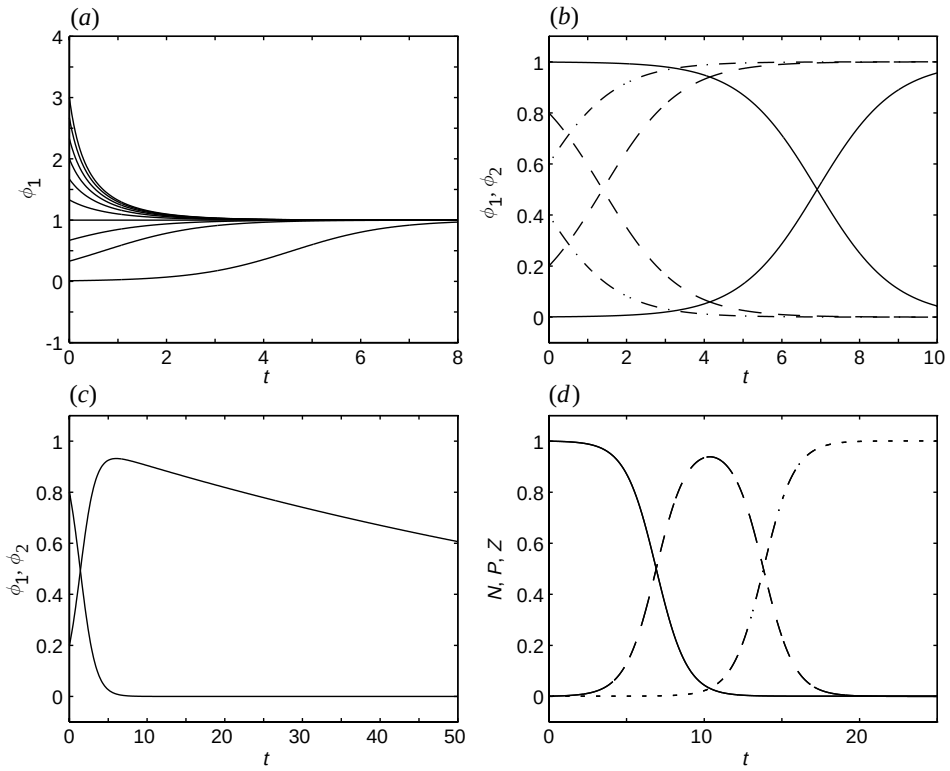

Figure 3. (*a*) Approach to carrying capacity (ϕ versus t for $\phi_{10} = (0.01, 0.33, 0.67, 1.0, 1.33, 1.67, 2.0, 2.33, 2.67, 3.0)$); (*b*) nonlinear conversion (ϕ_1, ϕ_2 versus t for $\phi_{10} = 0.999$ (solid), 0.8 (dashed), 0.4 (dash-dot)); (*c*) effect of mortality on the predator after the prey is depleted (ϕ_1, ϕ_2 versus t for $\phi_{10} = 0.8$, $\alpha_{20} = 0.01$); (*d*) N (solid), P (dashed), Z (dash-dot) versus t, $\epsilon = 0.001$.

(*c*) *Grazing*

To study grazing we non-dimensionalize the time by $t_0 = (a_{21}M)^{-1}$, with M as an arbitrary biomass density. Equations (4.1) become

$$\frac{\mathrm{d}\phi_1}{\mathrm{d}t} = \phi_1(\alpha_{10} - \hat{\alpha}_{11}\phi_1 - \phi_2), \tag{4.8\,a}$$

$$\frac{\mathrm{d}\phi_2}{\mathrm{d}t} = \phi_2(-\hat{\alpha}_{20} + \phi_1), \tag{4.8\,b}$$

where

$$\alpha_{10} = \frac{a_{10}}{a_{21}M} = \frac{C}{M}\hat{\alpha}_{11}, \quad \hat{\alpha}_{20} = \frac{\hat{a}_{20}}{a_{21}M} = \frac{G}{M}, \quad \hat{\alpha}_{11} = \frac{\hat{a}_{11}}{a_{21}}.$$

To present the stability results for the grazing equilibrium (4.4 *c*), we set $M = G$ or $\hat{\alpha}_{20} = 1$. Thus

$$\Phi_1 = 1; \quad \Phi_2 = \alpha_{10} - \hat{\alpha}_{11}, \quad \alpha_{10} > \hat{\alpha}_{11}, \tag{4.9\,a}$$

and δ, ϵ (equations (4.2)) satisfy the linearized equations

$$\frac{\mathrm{d}}{\mathrm{d}t}\delta = -\hat{\alpha}_{11}\delta - \epsilon, \tag{4.9\,b}$$

$$\frac{\mathrm{d}}{\mathrm{d}t}\epsilon = (\alpha_{10} - \hat{\alpha}_{11})\delta, \tag{4.9\,c}$$

For solutions $\sim \exp[\sigma t]$,

$$2\sigma = -\hat{\alpha}_{11} \pm [\hat{\alpha}_{11}^2 - 4(\alpha_{10} - \hat{\alpha}_{11})]^{1/2}, \quad \text{or} \tag{4.9 d}$$

$$= -\hat{\alpha}_{11} \pm 2(-\alpha_{10})^{1/2}, \quad \text{if } \alpha_{10} \gg \hat{\alpha}_{11}. \tag{4.9 e}$$

For $\hat{\alpha}_{11} \equiv 0$ this reduces to the neutrally stable oscillation of the classical Lotka–Volterra model with dimensional frequency $[a_{10}\hat{\alpha}_{20}]^{1/2}$. For all finite $\hat{\alpha}_{11}$ the grazing equilibrium is stable and for small $\hat{\alpha}_{11}$ the decay rate is given directly by $\hat{\alpha}_{11}$. The coefficients of the right-hand side of (4.9 *b*), (4.9 *c*) are the elements of the community matrix with trace and determinant

$$\mathrm{Tr} = -\hat{\alpha}_{11} < 0, \quad D = \alpha_{10} - \hat{\alpha}_{11} > 0, \tag{4.9 f}$$

and $(\mathrm{Tr})^2 = 4D$, when

$$\hat{\alpha}_1^* = 2(1 + \alpha_{10})^{1/2} - 2.$$

For $\hat{\alpha}_{11} \gtrless \alpha_{11}^*$ the grazing equilibrium is a stable node or stable spiral in phase space and $\hat{\alpha}_{11} = 0$ is a neutral centre. More generally, the grazing equilibrium has been shown to be globally stable in the Liapunov sense (Freedman 1980).

Next we present the solution for the nonlinear conversion of prey to predator for the limiting case that the grazing rate is much faster than growth and mortality rates. From equation (4.8) this limit is seen to require

$$M \gg G, \quad M \gg \hat{\alpha}_{11} C, \quad 1 \gg \hat{\alpha}_{11}. \tag{4.10 a}$$

Setting $\alpha_{10} = \hat{\alpha}_{11} = \hat{\alpha}_{20} = 0$ in (4.8) yields solutions

$$\phi_1 = \frac{\phi_{10}(\phi_{20} + \phi_{10})}{\phi_{10} + \phi_{20}\mathrm{e}^t}, \tag{4.10 b}$$

$$\phi_2 = \frac{\phi_{20}(\phi_{20} + \phi_{10})\mathrm{e}^t}{\phi_{10} + \phi_{20}\mathrm{e}^t}, \tag{4.10 c}$$

$$\phi_1 + \phi_2 = \phi_{10} + \phi_{20} = 1. \tag{4.10 d}$$

Asymptotically the total biomass (2.1) is in the predator ϕ_2. For specificity in the next section, we may regard $\phi_1 - \phi_2$ as a phytoplankton–zooplankton system or as a nutrient–phytoplankton system. Nonlinear conversion is illustrated in figure 3*b*.

The effect of mortality of the predator can be treated analytically via singular perturbation theory when the mortality rate is small but finite. Thus we keep $\alpha_{10} = \hat{\alpha}_{11} = 0$ but retain $\hat{\alpha}_{20} \ll 1$ in (4.8) as the perturbation parameter. The solution (4.10 *b*) for the prey is unaltered but the solution for the predator is now

$$\phi_2 = (\phi_{20} + \phi_{10}) \left[\frac{\phi_{20}\mathrm{e}^t}{\phi_{10} + \phi_{20}\mathrm{e}^t} + \mathrm{e}^{-\hat{\alpha}_{20} t} - 1 \right]. \tag{4.10 e}$$

The solution is uniformly valid in time under the condition $\hat{\alpha}_{20} < \phi_{20}$, and has been checked by numerical integration for selected parameters. An example is plotted on figure 3*c*.

Consider for example ϕ_1 as a chemical nutrient and ϕ_2 as phytoplankton. After consuming almost all the nutrient in the dimensional time scale $(a_{21}M)^{-1}$ the phytoplankton slowly die off on the dimensional time scale $(a_{21}G)^{-1}$, as shown on figure 3*c*. The plankton ϕ_2 asymptotically approach zero identically but there is a small residual amount of nutrient $\phi_{1\infty}$ which can be computed from the exact integral of the system. Equation (4.10 *d*) is now replaced by

$$\phi_1 + \phi_2 - \hat{\alpha}_{20} \ln \phi_1 = \phi_{10} + \phi_{20} - \hat{\alpha}_{20} \ln \phi_{10} = 1 - \alpha_{20} \ln \phi_{10} \doteq 1. \tag{4.10 f}$$

Since $\phi_{2\infty} = 0$ and $\phi_{1\infty}$ is small, we have

$$\phi_{1\infty} + \phi_{2\infty} - \hat{\alpha}_{20} \ln \phi_{1\infty} \doteq -\hat{\alpha}_{20} \ln \phi_{1\infty} \doteq 1, \tag{4.10 g}$$

whence

$$\phi_{1\infty} = \exp[-(\hat{\alpha}_{20})^{-1}]. \tag{4.10 h}$$

(*d*) *N–P–Z model*

The nonlinear conversion results are extended to a three-component system. The phytoplankton $\phi_1 = P$ are grazed by the zooplankton $\phi_2 = Z$ while they consume the nutrient $\phi_3 = N$. We assume perfect grazing ($a_{ij} = -a_{ji}$) and neglect mortalities ($a_{io} = a_{ii} = 0$). The non-dimensional model equations, with all biomasses scaled by M and $t_0 = (a_{13}M)^{-1}$, are

$$P_t = PN - \beta PZ, \tag{4.11 a}$$

$$Z_t = \beta PZ, \tag{4.11 b}$$

$$N_t = -PN. \tag{4.11 c}$$

This is a reduced form of the zero-dimensional NPZ model used by Klein & Steele (1985) as the basis for a numerical study of advective and diffusive effects in one and two spatial dimensions. They included nutrient recycling and uniform flow in idealized Georges Bank geometries.

The parameter $\beta = a_{21}(a_{13})^{-1}$, the ratio of the grazing interaction coefficients, measures the relative rate of zooplankton depletion of phytoplankton to their growth rate via nutrient consumption. Addition of the three equations and an integration after eliminating P from (4.11 *b*), (4.11 *c*), yields two integrals of the system

$$N + P + Z = \mathcal{B}, \tag{4.12 a}$$

$$ZN^{\beta} = \mathcal{C} \tag{4.12 b}$$

and a quadrature solution

$$\int \frac{\mathrm{d}N}{[-N^2 + \mathcal{B}N - \mathcal{C}N^{(1-\beta)}]} = -t. \tag{4.12 c}$$

Here $\mathcal{B}$, $\mathcal{C}$ are constants of integration.

To facilitate the study of advective effects we seek relatively simple solutions to the zero-dimensional biological dynamics. Thus we will take the exact solution for $\beta = 1$ and approximate solutions for general β. For $\beta = 1$, (4.12 *c*) integrates to

$$N = \frac{\mathcal{E}(\mathcal{B} - \mathcal{D}) + (\mathcal{B} + \mathcal{D})\mathrm{e}^{-\mathcal{D}t}}{2(\mathcal{E} + \mathrm{e}^{-\mathcal{D}t})}, \tag{4.12 d}$$

$$\mathcal{D} = (\mathcal{B}^2 - 4\mathcal{C})^{1/2},$$

which together with (4.12 *a*), (4.12 *b*) completes the solution. $\mathcal{E}$ is the third integration constant. In terms of the three initial values of biomass at $t = 0$,

$$\mathcal{B} = N_0 + P_0 + Z_0, \quad \mathcal{C} = N_0 Z_0, \quad \mathcal{E} = \frac{\mathcal{B} + \mathcal{D} - 2N_0}{2N_0 - (\mathcal{B} - \mathcal{D})}. \tag{4.12 e}$$

A case of special interest is that in which the biomass is initially almost entirely in the nutrient with equal small background values of planktons. Then

$$N_0 = O(1), \quad P_0 = Z_0 = \epsilon \ll 1 \tag{4.12 f}$$

and

$$\mathcal{B} = N_0 + 2\epsilon, \quad \mathcal{C} = \epsilon N_0, \quad \mathcal{D} = N_0, \quad \mathcal{E} = \frac{\epsilon}{N_0}, \tag{4.12 g}$$

to accuracy $O(\epsilon)$. Asymptotically in time

$$Z_\infty = N_0 + \epsilon, \quad N_\infty = \epsilon, \quad P_\infty = 0. \tag{4.12 h}$$

With equal grazing rates almost the entire nutrient supply is successfully converted into zooplankton. This solution is shown on figure 3*d* for $N_0 = 1$.

If $\beta = 0$, the system reduces to the two components (N, P) and the solution becomes

$$N = \frac{N_0(N_0+\epsilon)\mathrm{e}^{-\mathcal{B}t}}{N_0\mathrm{e}^{-\mathcal{B}t} + \epsilon}, \quad P = \frac{\epsilon(N_0+\epsilon)}{N_0\mathrm{e}^{-\mathcal{B}t} + \epsilon}, \tag{4.12 i}$$

$$\mathcal{B} = N_0 + \epsilon, \quad P_\infty = N_0, \quad N_\infty = 0,$$

as for equations (4.10) and figure 3*b*.

From (4.11 *a*) we note that the initial rate of plankton growth is given by $P_0(N_0 - \beta Z_0)$. Thus if $\beta \ll 1$, N_0 will first be converted to P via the two-component process described by equation (4.12 *i*), followed by a similar two-component conversion of N_0 to Z but on the longer time scale β^{-1}. For $\beta > N_0 Z_0^{-1}$, P decreases immediately at $t = 0$ and cannot efficiently act as a conduit for the growth of Z. For $\beta > N_0 Z_0^{-1}$ Z can only convert P_0, and asymptotically $N_\infty = N_0$, $P_\infty = 0$, $Z_\infty = Z_0 + P_0$. Thus rapid grazing is disadvantageous for the zooplankton.

An interesting case lies in the determination of asymptotic values in the range $N_0 Z_0^{-1} > \beta > 1$; for conditions (4.12 *f*) this becomes $\beta < O(\epsilon^{-1})$. There is an initial growth of plankton to a maximum value P_m with associated values Z_m, N_m, at $t = t_\mathrm{m}$. From (4.11 *a*) $N_\mathrm{m} = \beta Z_\mathrm{m}$ when $P_t = 0$. From (4.12 *a*), (4.12 *b*), (4.12 *f*)

$$N + P + Z = N_0 + 2\epsilon, \quad N = N_0 \epsilon^{(1/\beta)} Z^{-(1/\beta)}, \tag{4.13 a}$$

$$Z_\mathrm{m} = \epsilon^{(1/1+\beta)} \beta^{-(\beta/1+\beta)} N_0^{(\beta/1+\beta)} \tag{4.13 b}$$

and N_m, P_m are given by (4.13 *a*). After the maximum the asymptotic values are approached rapidly in the now faster time scale β^{-1}. Inspection of (4.12 *a*), (4.12 *b*), (4.12 *c*) shows $P_\infty = 0$, and the exact asymptotics can be then computed from (4.13 *a*).

$$(N_0 + 2\epsilon - N_\infty) N_\infty^\beta = \epsilon N_0^\beta, \quad Z_\infty = N_0 + 2\epsilon - N_\infty \tag{4.13 c}$$

or

$$N_\infty = \epsilon^{1/\beta} N_0^{1-1/\beta}, \quad \epsilon \ll 1.$$

Given the exact values of the state variables at the maximum and at ∞, the solution can be completed approximately by using a two-component N–P conversion (4.12 *i*) up to the maximum and a two-component P–Z conversion beyond the maximum. Table 1 presents some numerical values for the fields at t_m and for the asymptotic partitioning of N_0 between Z_∞ and N_∞.

5. Interactive processes

In this section we consider the occurrence of the biological processes of the previous section in the presence of a dynamically interesting flow field with deformation. We will present results for the competition between physical and biological effects for: the

Table 1. *Field values at the maximum and at infinity*

ϵ	β	Z_{m}	N_{m}	P_{m}	Z_{∞}	N_{∞}
0.0010	5.0000	0.0827	0.4135	0.5058	0.7508	0.2512
0.0010	10.0000	0.0658	0.6579	0.2783	0.5008	0.5012
0.0010	15.0000	0.0513	0.7691	0.1816	0.3710	0.6310
0.0010	100.0000	0.0098	0.9775	0.0148	0.0687	0.9333
0.0100	5.0000	0.1214	0.6070	0.2916	0.6219	0.3981
0.0100	10.0000	0.0811	0.8111	0.1278	0.3890	0.6310
0.0100	15.0000	0.0592	0.8882	0.0726	0.2844	0.7356

stability analyses; the nonlinear approach to carrying capacity or advective equilibria; and nonlinear grazing.

The parameter $\alpha = u_0 t_0 L^{-1}$ (equation (2.10 *c*)) measures the relative importance of advective to biological effects if t_0 is chosen as the characteristic time of the dominant biological process. As for equations (3.4) we choose $v_1 = u_2 = 0$ in (3.2) and set $u_0 L^{-1} = u_1$, the deformation gradient of the flow field $\psi = -u_1 xy$. Equations (2.10), (2.11), (2.12) in non-dimensional form appear as

$$\frac{\partial \phi_i}{\partial t} + \alpha \left[x \frac{\partial \phi_i}{\partial x} - y \frac{\partial \phi_i}{\partial y} \right] = B_i(\phi_j), \tag{5.1 a}$$

$$\frac{\mathrm{d}t}{\mathrm{d}s} = 1, \quad \frac{\mathrm{d}x}{\mathrm{d}s} = \alpha x, \quad \frac{\mathrm{d}y}{\mathrm{d}s} = -\alpha y, \quad \frac{\mathrm{d}\phi_1}{\mathrm{d}s} = B_i, \tag{5.1 b}$$

$$\alpha = u_1 t_0, \quad \alpha_{i0} = t_0 a_{i0}, \quad \alpha_{ij} = M t_0 a_{ij} \quad \text{and} \quad \psi = -xy.$$

Note that because of the special form of the velocity field, L does not appear in α. The biological operator has been scaled by $M t_0^{-1}$. Again we will treat the initial value problem in the time domain so the solutions (2.14 *b*) are

$$s = t, \quad r = x\mathrm{e}^{-\alpha s}, \quad q = y\mathrm{e}^{\alpha s}. \tag{5.1 c}$$

Since gradients in the direction of the axis of contraction (dilation) amplify (decay) it suffices to take the initial condition as a function of y only, i.e.

$$\phi_i(x, y, t = 0) = \phi_i(q(y, 0), 0) = \phi_i(y, 0), \tag{5.1 d}$$

which for a local gradient analysis will be as in (3.1 *a*) with $c_1 = 0$, i.e.

$$\phi_i(y, 0) = \gamma_{0i} + \gamma_{2i} y\mathrm{e}^{\alpha t} \tag{5.1 e}$$

$$\gamma_{0i} = \frac{c_{0i}}{M}, \quad \gamma_{2i} = \frac{c_{2i} L}{M}$$

in non-dimensional form.

(*a*) *Linearized instabilities of equilibria*

Since $\alpha > 0$ always, $q = y\mathrm{e}^{\alpha t}$ represents exponential growth, and the presence of an initial spatial gradient of ϕ_i can significantly alter stability properties in the presence of the physical flow. Stable solutions can be rendered unstable and instabilities will occur with enhanced growth rates.

Table 2. *Destabilizing shears*

state	α	condition		effect
null	$u_1 a_{10}$	$\alpha > \hat{\alpha}_{20}$ or	$u_1 > a_{20}(a_{10})^{-2}$	predator unstable
carrying capacity	$u_1 a_{10}$	$\alpha > 1$	$u_1 > (a_{10})^{-1}$	instability
grazing	$u_1 \hat{a}_{20}$	$2\alpha > \hat{\alpha}_{11}$	$u_1 > \hat{a}_{11}(a_{21}\hat{a}_{20})^{-1}$	instability

Linearity allows separability, thus

$$\phi_i = d_i(q)\phi_i^0(t) = (\gamma_{0i} + \gamma_{2i} y \mathrm{e}^{\alpha t})\phi_i^0(t), \tag{5.2}$$

The $\phi_i^0(t)$ are the zero-dimensional biological dynamical solutions for the null (n), carrying capacity (c) and grazing (g) states (equations (4.4)) whose stability properties are given by equations (4.6)–(4.7), (4.9). In those solutions, e.g. (4.6), the initial conditions δ_0, ϵ_0 are now replaced by $d_1(q)$, $d_2(q)$ from (5.2).

For the null state (4.6) the instability of the prey is enhanced and the stability of the predator can be switched to instability if the advective supply rate exceeds the decay rate. Sufficient advection can also destabilize both the carrying capacity (4.7) and grazing states (4.9); the Lotka–Volterra model in the presence of deformation advection is always switched from neutral stability to instability. The quantitative conditions among the biological rate and interaction parameters and the deformation shear are given in table 2.

Okubo (1980, ch. 10) reports a stabilization of the Lotka–Volterra model when the predator and prey tend to migrate towards a central favourable region with constant velocities in the presence also of diffusion.

(*b*) *Carrying capacity versus advective equilibria*

Here we consider the behaviour of the one component biological system, e.g. phytoplankton (4.7), in the presence of the deformation advection of equation (5.1). The solutions are now given by (4.7 *c*), (4.7 *d*) with δ_0, ϕ_{10} replaced by functions of q as in (5.1 *c*).

First we generalize the stability analysis of equation (5.2) for case $\gamma_0 = 0$, $\gamma_2 = 1$. Now $M = C$ and $L = Cc_2^{-1}$. The nonlinear solution for the departure from equilibrium is

$$\delta = \begin{cases} \dfrac{d}{(d+1)\mathrm{e}^t - d}, & y > y_0 = -\mathrm{e}^{-\alpha t}, \\ -1, & y < y_0 = -\mathrm{e}^{-\alpha t}, \end{cases} \tag{5.3 a}$$

$$d = y\mathrm{e}^{\alpha t}. \tag{5.3 b}$$

The initial ($t = 0$) population is null for $y < -1$ and varies linearly with y for $y > -1$, passing through the carrying capacity equilibrium value at $y = 0$.

The limit of pure advection is given by $\delta = d$ directly by (5.3 *b*) or equivalently by setting $\mathrm{e}^t = 1$ in (5.3 *a*) but retaining $\mathrm{e}^{\alpha t}$. The limit of pure biology is given by $\alpha = 0$. Both of these limits are plotted on figure 4*a*. Advection is plotted for $\alpha = 1$, i.e. with equal advective and biological time scales. To interpret these and subsequent plots note that at $t = 0$, $\delta = y$, so that a curve emanating from a point δ^* on the ordinate axis represents $\delta(y = \delta^*, t)$. The biological behaviour is of course identical to that

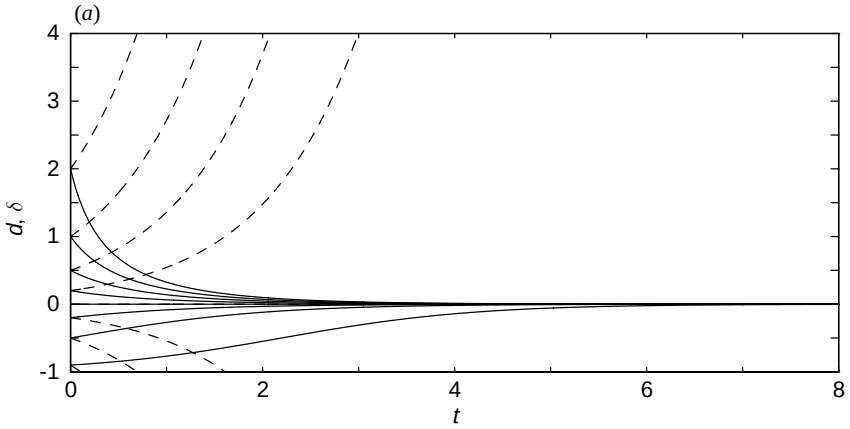

Figure 4. Carrying capacity versus advective equilibria: (*a*) δ versus t for $\alpha = 0$ (solid, pure biology) and d versus t for $\alpha = 1$ (dashed, pure advection).

shown on figure 3*a*. The advective solutions for $y > 0$ amplify indefinitely but for $y < 0$ reach the limiting value $\delta = -1$ at time $t_{-1} = \ln(-y^{-1})$ and remain at that value thereafter. This behaviour is consistent with the deformation flow (see figure 2*b*) ultimately advecting in fluid with no phytoplankton for $y < 0$ but advecting in fluid with an ever increasingly dense population for $y > 0$.

The general interactive solution is illustrated on figure 4*b* for values of $\alpha = (0.1, 1, 10)$ which range from relatively weak to strong advective effects and span all qualitative behaviours. The solutions equation (5.3 *a*) have maxima at $t = t_{\mathrm{m}}$ for both positive and negative y but only for a range of values. The times at which maxima and limiting values are reached are

$$t_{\mathrm{m}} = \frac{1}{\alpha} \ln\left(\frac{\alpha - 1}{y}\right),$$

$$\left.\begin{array}{llll} y > 0, & \alpha > 1, & y < \alpha - 1, \\ y < 0, & \alpha < 1, & y < \alpha - 1, \end{array}\right\} \tag{5.3 c}$$

and

$$t_{-1} = \frac{1}{\alpha} \ln\left(-\frac{1}{y}\right).$$

Asymptotically in time an excess initial population always approaches the carrying capacity equilibrium but a deficit population approaches the advective null equilibrium.

Examination of figure 4*b* shows some interesting effects. Frontogenesis occurs, ultimately producing a very sharp front of unit strength. For large α and positive y, advection dominates until the maximum is reached at t_{m} and a much stronger but broader front is present. For large α and negative y advection dominates with but little biological modification before t_{-1}. For small α, advection has little effect on the approach to the biological equilibrium for positive y. For negative y and small α, however, the solutions are dominated by almost pure biological behaviour for a long time, i.e. until $t_{\mathrm{m}} \gg 1$. Biological equilibrium is very nearly achieved whence advection suddenly sweeps away the population. This is because (equations (5.3))

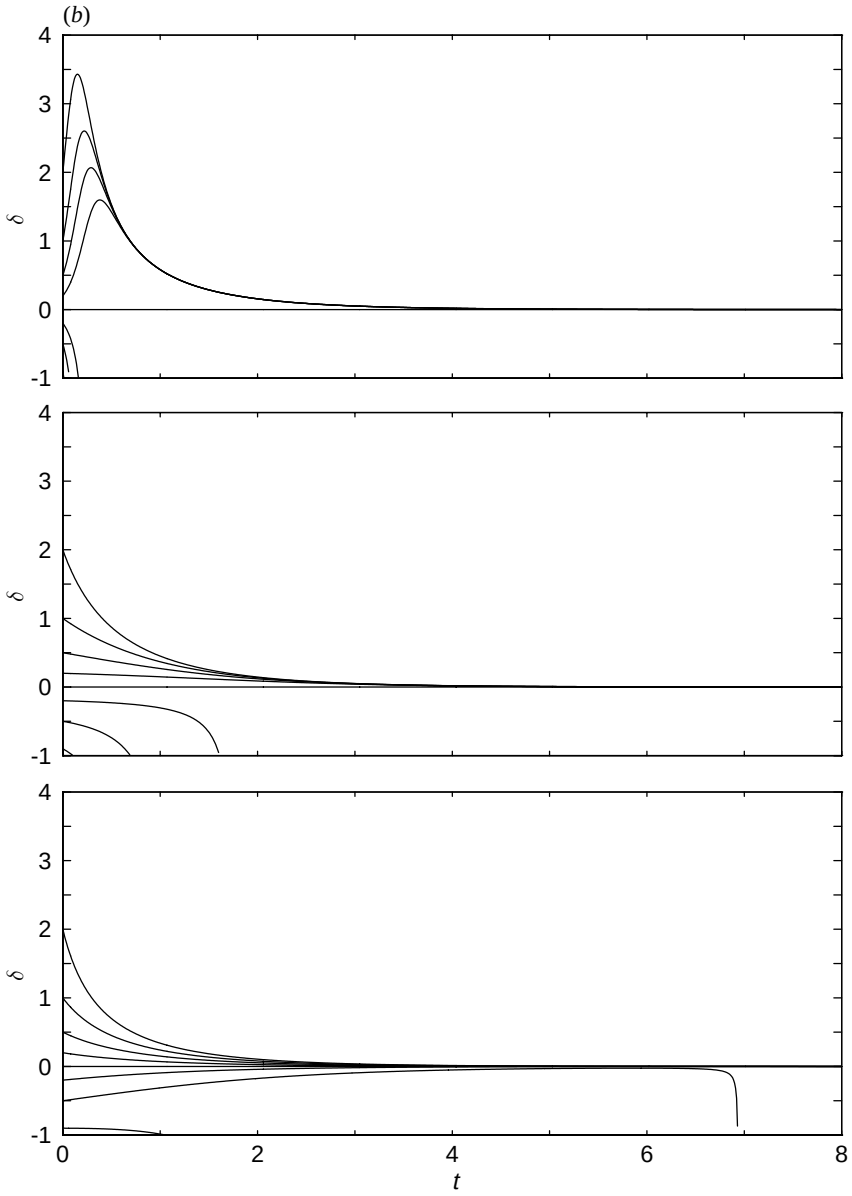

Figure 4. Carrying capacity versus advective equilibria. (*b*) Dependance on relative strength of advection: top, δ versus t for $\alpha = 10$; middle, δ versus t for $\alpha = 1$; bottom, δ versus t for $\alpha = 0.1$.

for $\alpha \ll 1$, $t_{\mathrm{m}} \approx t_{-1}$. The curve emanating at $y = -0.20$ for $\alpha = 0.10$ which is indistinguishable from zero at $t = 8$ has the associated values $t_{\mathrm{m}} = 15.04$, $t_{-1} = 16.09$.

The next problem deals with the identical dynamics as the previous one but for the initial condition introduces a finite frontal width L across which the biomass density changes from zero to a maximum value of F. We retain the biomass scaling $M = C$ as introduced prior to equation (5.3 *a*). The initial condition is now taken as

$$\phi_1(y, 0) = \gamma(1 + \tanh y), \quad \gamma = \frac{F}{2C}, \tag{5.4 a}$$

$$\phi_1(y,0) = \gamma(1+y), \quad y \ll 1,$$

$$\phi_1(\infty,0) = 2\gamma, \quad \phi_1(0,0) = \gamma, \quad \phi_1(-\infty,0) = 0.$$

The cross frontal coordinate has been scaled by L, recall that $\tanh(2) = 0.96$. Note that in the vicinity of the y-origin this solution will correspond to that of the preceding section if $\gamma = 1$.

The approach to equilibrium is now given by

$$\phi_1 = \frac{d_1}{d_1 + (1-d_1)\mathrm{e}^{-t}} = \frac{1}{1 + (1/d_1 - 1)\mathrm{e}^{-t}}, \tag{5.4 b}$$

$$d_1 = \gamma(1 + \tanh y\mathrm{e}^{\alpha t}). \tag{5.4 c}$$

Since d_1 remains finite for all time for $y \geqslant 0$, the asymptotic behaviour is a simple exponential decay in time to the biological equilibrium $\phi_1 = 1$. For negative y, d_1 approaches zero as

$$\phi_1 = 2\gamma \exp(2y\mathrm{e}^{\alpha t} + t), \quad y < 0, \quad t \to -\infty. \tag{5.4 d}$$

The interpretation, illustrated below, is that for $y < 0$ the asymptotic limit is always a decay to the advective null equilibrium, but that before a time t_a determined by

$$t_\mathrm{a}\mathrm{e}^{-\alpha t_\mathrm{a}} = -2y, \tag{5.4 e}$$

there can be a growth towards the biological equilibrium unity, which can be approached very closely for $\alpha < 1$. Note that for $\gamma < 0.5$ the initial condition is everywhere a deficit of population density from the carrying capacity. As advection tightens the front across $y = 0$, the excess or deficit of density advected in from the populated side of the front is adjusted by biological processes to the carrying capacity.

The range of qualitative behaviour of solution (5.4) as a function of the relative rate and frontal strength parameters (α, γ) is illustrated on figure 5. Figure 5*a* presents the pure biological and pure advective limits. Figures 5*b*, *c* are for an initial frontal strength (2γ) somewhat larger than the carrying capacity and figures 5*d*, *e* show the behaviour for a weaker (stronger) front. Figure 5*c* illustrates a small α behaviour analogous to that on figure 4*b*.

(*c*) *Grazing with advection*

The effects of advection on grazing are particularly interesting since advective supply of nutrients can dominate the qualitative and quantitative behaviour of the biological dynamics. We retain the deformation flow field of equation (5.1). For definiteness of interpretation, we can consider solutions in the half-plane $y > 0$ as representing an infinitely deep ocean with sea surface at $y = 0$. Thus advection can be regarded as bringing material from the deep sea into the surface region. The models remain of course highly ideaized and we do not intend to imply any direct realistic oceanic relevance.

The advective process introduces a new advective equilibrium state. Introducing the biology of equations (4.10) into equations (5.1 *a*), (5.1 *b*) and setting $(\partial/\partial t) = (\partial/\partial x) = 0$ yields

$$-\alpha y \frac{\partial P}{\partial y} = PN, \tag{5.5 a}$$

$$-\alpha y \frac{\partial N}{\partial y} = -PN, \tag{5.5 b}$$

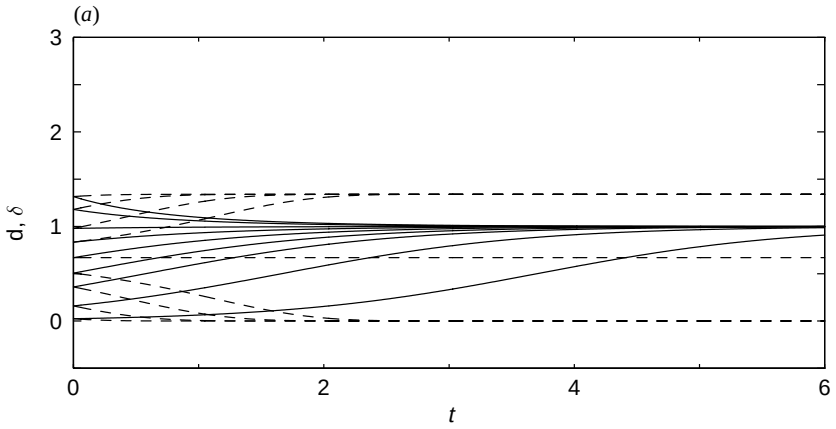

Figure 5. As for figure 4 but for a finite front. (*a*) ϕ for $\alpha = 0$ (solid, pure biology); d versus t for $\gamma = 0.67$, $\alpha = 1$ (dashed, pure advection).

with solutions

$$N = \frac{\mathcal{B}}{1 + \mathcal{A}\mathrm{e}^{-(\mathcal{B}/\alpha)\ln y}}, \tag{5.5 c}$$

$$P = \frac{\mathcal{A}\mathcal{B}\mathrm{e}^{-(\mathcal{B}/\alpha)\ln y}}{1 + \mathcal{A}\mathrm{e}^{-(\mathcal{B}/\alpha)\ln y}}, \tag{5.5 d}$$

$$N + P = \mathcal{B}, \tag{5.5 e}$$

where $\mathcal{A}$, $\mathcal{B}$ are pure constants of integration. $\mathcal{B}$ is the biomass at $y = \infty$, where $P = 0$. When $y = 0$, $P = \mathcal{B}$ and $N = 0$; when $y = 1$, $N = \mathcal{B}(1 + \mathcal{A})^{-1}$. The structure of the nutricline can be seen on figure 6 to depend upon $\mathcal{A}$ but to be primarily controlled by α. The advecting velocity, the source at infinity, and the geometry require a specific spatial distribution of biological fields. Advective equilibria are an important aspect of physical–biological interactions in the sea, but are not the focus of this study. We mention the solution (5.5) for completeness but return to our central theme which is to introduce deformation flow advection into the nonlinear grazing dynamics of equations (4.10), (4.12), (4.13).

We need consider only equations (4.11)–(4.13) since they contain the dynamics of (4.10) for the case of $\beta = 0$. For all solutions we will take the initial plankton fields as a small uniform background constant. The initial nutrient field will be a linear increase of N with depth y, and interest will be restricted to order unity depths. Thus

$$N(0) = 1 + y, \quad Z(0) = P(0) = \epsilon \tag{5.6 a}$$

and the advective solutions are given by (4.12), (4.13) with

$$N_0(r, q) = 1 + q = 1 + y\mathrm{e}^{\alpha t}, \tag{5.6 b}$$

$$N_0 = y\mathrm{e}^{\alpha t}, \quad t \to \infty,$$

from (5.1 *c*), (5.1 *d*). The asymptotic values for the two- and three-component systems are now given by (4.12 *i*), (4.12 *h*) and (4.13 *c*) with N_0 given by (5.6 *b*).

For the two-component NP system figure 7 illustrates the dependence of the grazing on the initial condition (ϵ) and the advective parameter (α). Figure 7*a* shows an initial advective growth of P followed by a complete depletion via grazing. It is

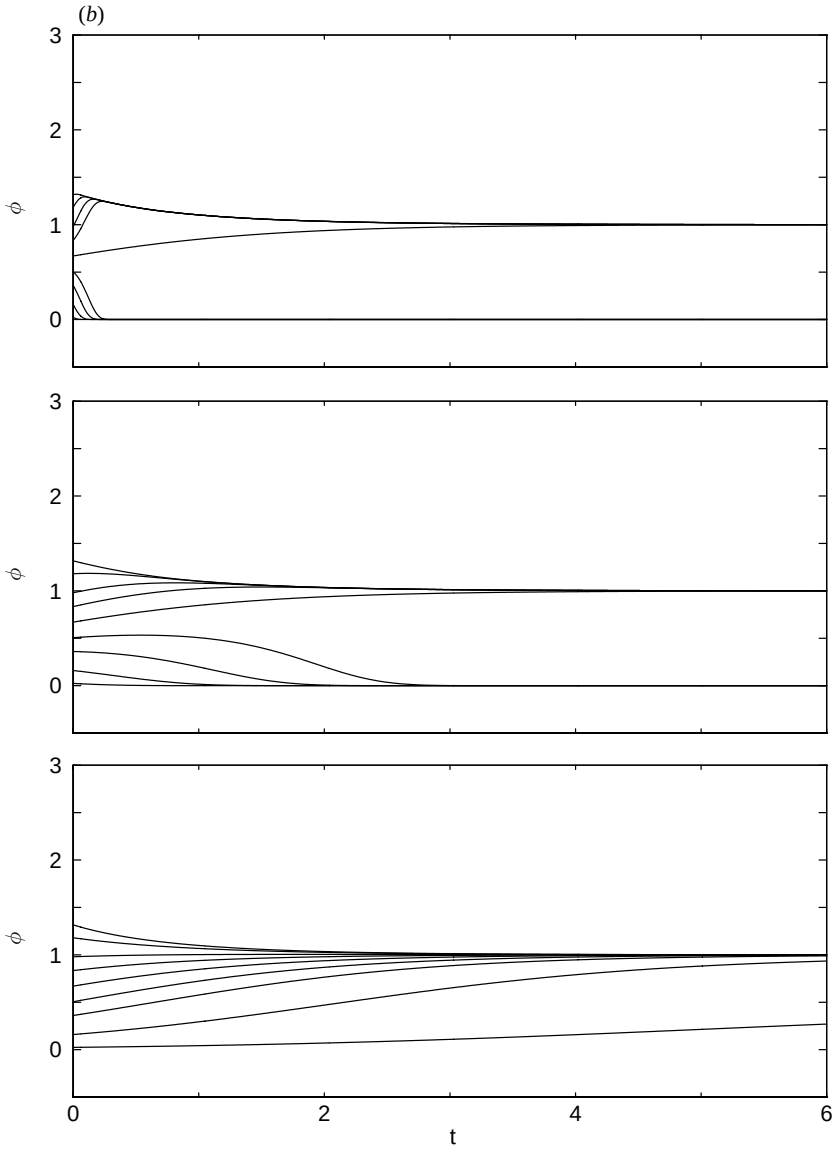

Figure 5. As for figure 4 but for a finite front. (*b*) Initial frontal strength somewhat larger than carrying capacity and show, respectively, the short-time behaviour: top, ϕ versus t for $\gamma = 0.67$, $\alpha = 10$; middle, ϕ versus t for $\gamma = 0.67$, $\alpha = 1$; bottom, ϕ versus t for $\gamma = 0.67$, $\alpha = 0.1$.

important to note that after some times the solution is independent of the value of the initial phytoplankton biomass, which simply controls the amplitude and time of occurrence of the maximum of N. Figures $7b, c$ for fixed $\epsilon = 0.001$ illustrates the dependence on the advection rate. Rapid advection results in an early large-amplitude maximum in N and an early rapid growth of P asymptotically.

Recall that if there were no planktons ($Z = P \equiv 0$) the purely advective solution for the inert passive nutrient would be given by (5.6 *b*) (see equation (3.4 *b*)). In the advective NP system ($\beta = 0$) for large t

$$P_\infty = N_0 = y\mathrm{e}^{\alpha t}, \quad N_\infty = 0, \tag{5.6 c}$$

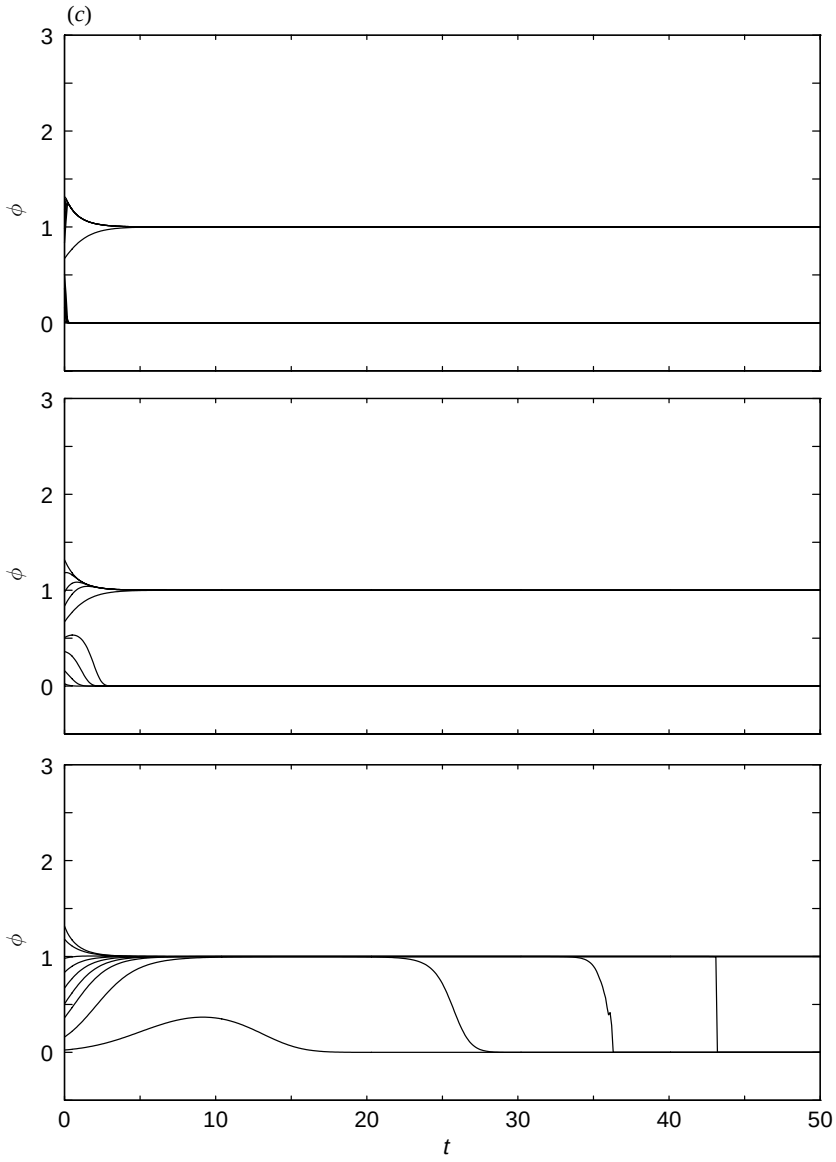

Figure 5. As for figure 4 but for a finite front. (*c*) Initial frontal strength somewhat larger than carrying capacity and show, respectively, the long-time behaviour: top, ϕ versus t for $\gamma = 0.67$, $\alpha = 10$; middle, ϕ versus t for $\gamma = 0.67$, $\alpha = 1$; bottom, ϕ versus t for $\gamma = 0.67$, $\alpha = 0.1$.

indicate that the phytoplankton effectively utilize all of the advected nutrient and continue to grow and accumulate an indefinitely large biomass in the upper ocean with no observable nutrient present. The local time derivative (equations (4.12 *i*), (5.6 *b*))

$$\left(\frac{\partial P}{\partial t}\right)_{x,y} = \left(\frac{\partial P}{\partial t}\right)_{N_0} + \left(\frac{\partial P}{\partial N_0}\right)_t \left(\frac{\partial N_0}{\partial t}\right) = NP + \alpha y \frac{\partial P}{\partial y} = \mathtt{G} + \mathtt{A} \qquad (5.6\,d)$$

$$= \frac{\epsilon N_0 (N_0+\epsilon)^2 \mathrm{e}^{Bt}}{(N_0+\epsilon \mathrm{e}^{Bt})^2} + \frac{\epsilon \mathrm{e}^{Bt}}{(N_0+\epsilon \mathrm{e}^{Bt})^2}[\epsilon(\mathrm{e}^{Bt}-1) + tN_0(N_0+\epsilon)]\alpha y \mathrm{e}^{\alpha t}$$

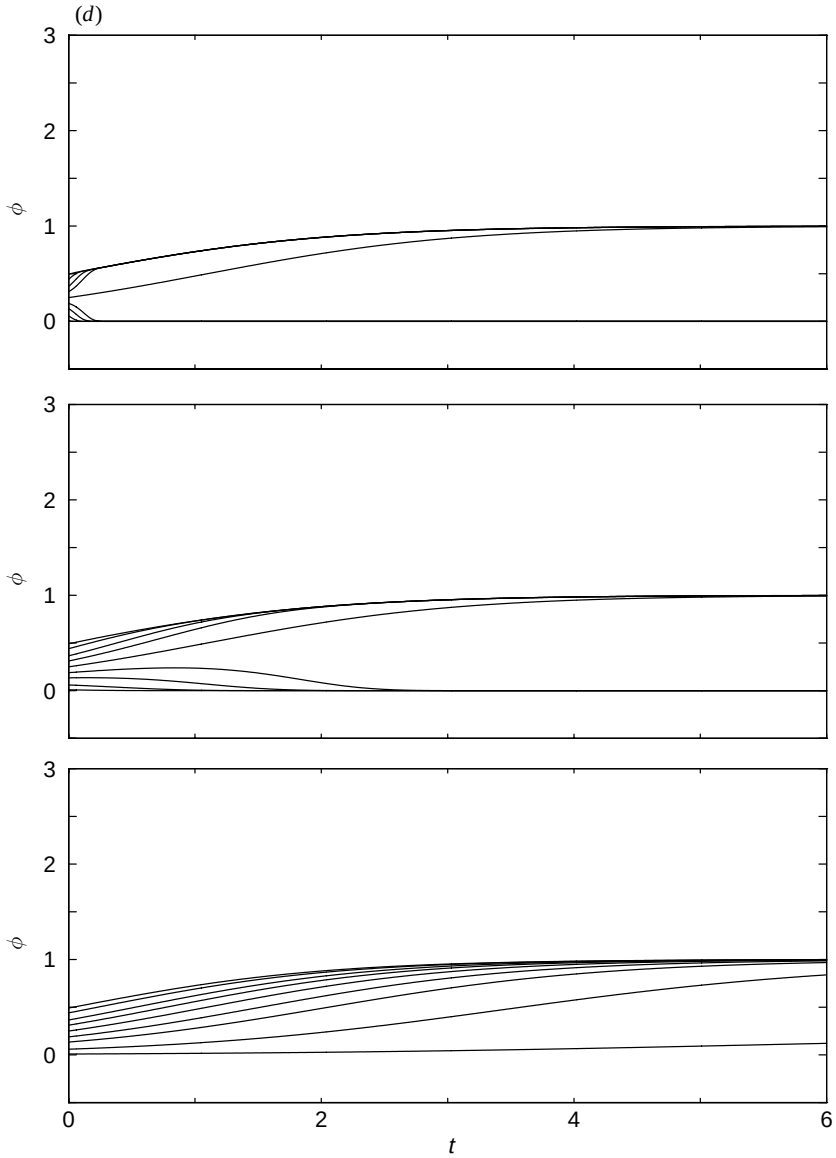

Figure 5. As for figure 4 but for a finite front. (*d*) Initial frontal strength smaller than carrying capacity: top, ϕ versus t for $\gamma = 0.25$, $\alpha = 10$; middle, ϕ versus t for $\gamma = 0.25$, $\alpha = 1$; bottom, ϕ versus t for $\gamma = 0.25$, $\alpha = 0.1$.

has a contribution from local grazing, `G`, and advective flux, `A`. These contributions are plotted versus time on figure 7*d*. At a given depth (y) local grazing has a maximum and then decays to zero; advective flux peaks, decays and then grows asymptotically. At greater depths, the extrema occur earlier and the maxima are larger. Thus the asymptotic growth of Z at a given depth is due to an advective flux from a grazing conversion which occurred earlier and deeper. The character of the solutions at very large times and depths is only of mathematical interest. Biological interpretations should be restricted to finite ranges of (y, t).

The behaviour of the three-component NPZ system for equal grazing rates ($\beta = 1$)

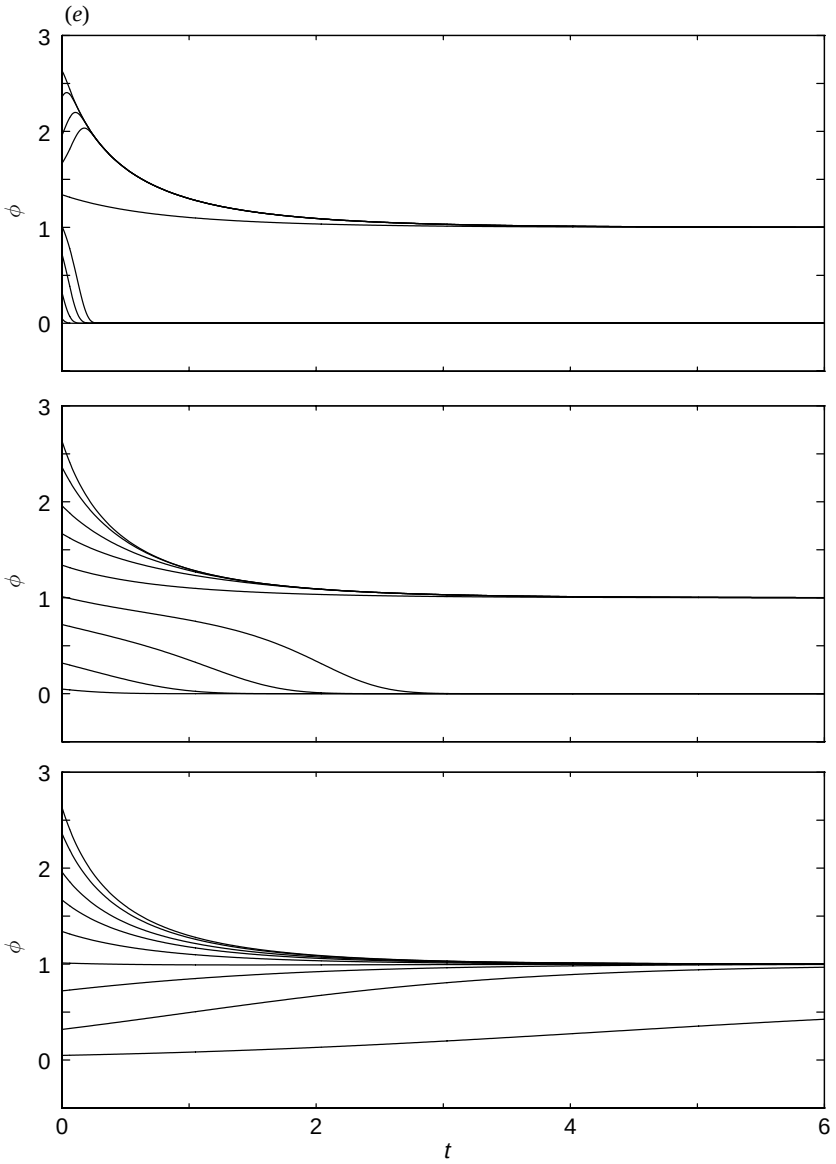

Figure 5. As for figure 4 but for a finite front. (*e*) Initial frontal strength much larger than carrying capacity: top, ϕ versus t for $\gamma = 1.34$, $\alpha = 10$; middle, ϕ versus t for $\gamma = 1.34$, $\alpha = 1$; bottom, ϕ versus t for $\gamma = 1.34$, $\alpha = 0.1$.

is shown on figures $8a, b$ for the same values of ϵ and α and the same scales as figures $7b, c$ for comparison. As indicated by equation $(4.12\,h)$, the advected nutrient is now asymptotically completely converted to Z with ultimately no observable N or P. The rate of the processes again increases with increasing α, as do the amplitudes of the successive maximum values of N and P. For $\beta \gg 1$, $1 \geqslant \epsilon\beta$, the fraction of nutrient effectively utilized by P and Z and its partioning between them, is given by $(4.13\,c)$. N and Z will now both be observed to grow exponentially after the initial adjustment time. In this model, rapid grazing by zooplankton leads to a smaller Z biomass than slow grazing.

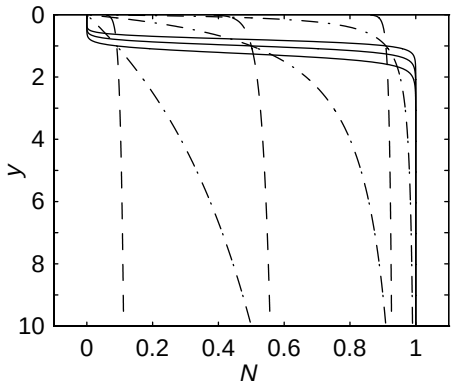

Figure 6. Advective equilibrium profiles ($\alpha = 0.1$ (solid), 1 (dash-dot), 10 (dashed)) (N versus y for $A = [0.1, 1, 10]$, $B = 1$). The A dependence is indicated by where the alpha triplets intersect at $y = 1$. For $A = (0.1, 1, 10)$, the intersections at $y = 1$ are at $N = (0.9, 0.5, 0.09)$, respectively.

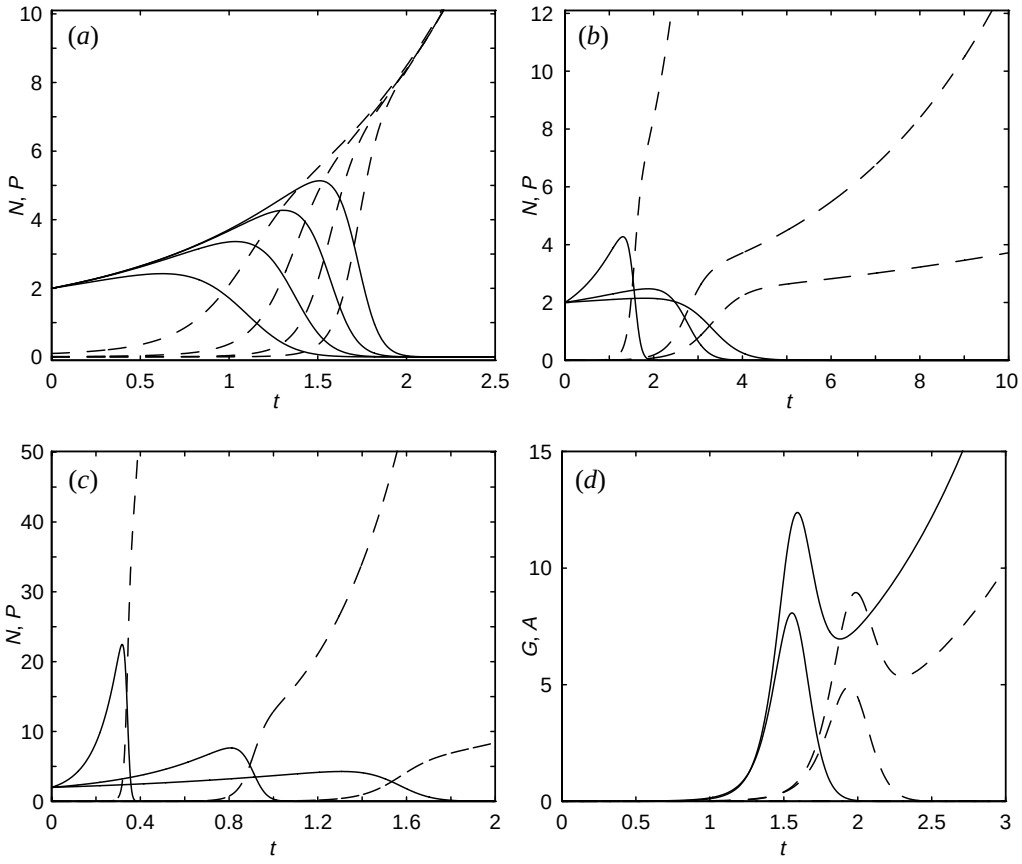

Figure 7. NP conversion (N, solid; P, dashed): (a) Dependence on initial conditions (N, P versus t for $y = 1$, $\epsilon = (0.1, 0.01, 0.001, 0.0001)$ $\alpha = 1$); (b) weak and moderate advection (N, P versus t for $y = 1$, $\alpha = (0.1, 0.25, 1.0)$ $\epsilon = 0.001$); (c) moderate and strong advection (N, P versus t for $y = 1$, $\alpha = (1.0, 2.5, 10)$ $\epsilon = 0.001$) as α increases, the maximum in N increases and the conversion to P occurs earlier (N, P versus t for $y = 1$, $\epsilon = 0.001$); (d) grazing and advection rates ($y = 0.5$ (dashed), 1.0 (solid), $\epsilon = 0.001$), as time increases local grazing stops.

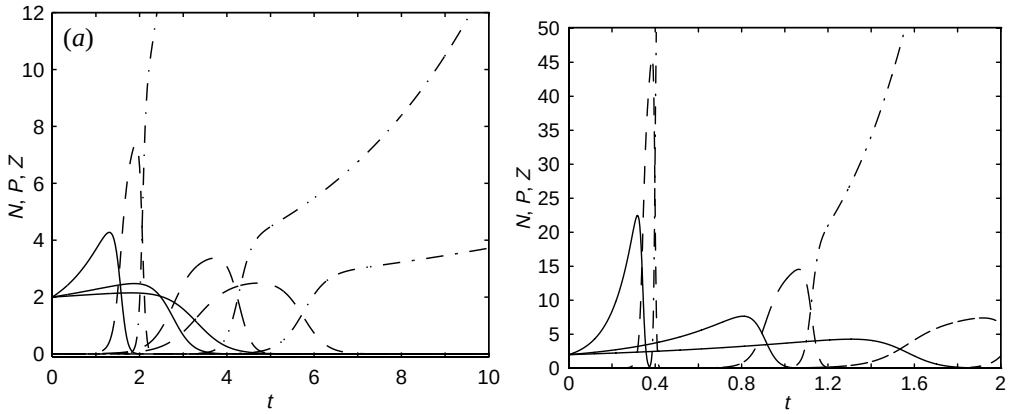

Figure 8. NPZ conversions (N, solid; P, dashed; Z, dash-dot): (a) weak and moderate advection (N, P, Z versus t for $y = 1$, $\epsilon = 0.001$, $\alpha = (0.1, 0.25, 1.0)$) ($b$) moderate and strong advection, maxima in N and P increase with increasing α and the rapid growth of Z occurs earlier (N, P, Z versus t for $y = 1$, $\epsilon = 0.001$, $\alpha = (1.0, 2.5, 10)$).

6. Summary and conclusions

This study presents a general theoretical structure for the analysis of advective effects on biological dynamics in the sea. It is based upon the mathematical theory of characteristics and, in the domain of the parameter s, involves the zero-dimensional local biological dynamics, as well as the Lagrangian trajectories of the fluid particles. The s-domain initial-value problems solved here were for the case that s was identified with the time t, and involved the specification of space-wise initial fields at $t = 0$. More general problems are possible and should be considered.

A kinematical analysis of the flow field was introduced and the effects of divergence, vorticity, stretching and shearing deformations on local gradients of biological state variables were discussed. The stretching deformation flow, which contains frontogenesis and frontolysis effects that contract and dilate gradients, was selected for the present study. The biological dynamical system included net birth or mortality, self-interactions and coupled-field interactions. Biological processes subjected to advection included: the approach to local equilibria; the stability or instability of equilibrium states for one-, two- or three-component systems; and nonlinear grazing conversions for NP and NPZ models. Further research should be directed towards additional and more realistic flow structures (vorticity, divergence, three dimensions, time-dependence and non-local circulation structures, etc.) as well as additional and more realistic biology (Michaelis–Menten grazing, light limitation, behaviour, etc.).

Advection by a deformation shear field in the presence of local gradients of the biological state variables was found capable of destabilizing null, carry-capacity and grazing equilibria and the velocity shear required was obtained in terms of the biological growth (death) rates and interaction coefficients. The competition between local biological and advective equilibria in the presence of frontogenesis was illustrated both for a simple deformation field flow and for a front of finite width. For an NPZ model the concept of advective-grazing equilibria was introduced and exemplified. For the cases of initial small background distribution of planktons in the presence of a deep ocean reservoir of nutrient the growth and conversion of planktons were calculated including the asymptotic in time partitioning of the advective nutrient input among the NPZ variables. At large times, P does not survive and Z is most successful by slow rather than rapid grazing.

These first results indicate the utility of the approach and provide some insight for further research. Deformation fields occur over a range of scales in the ocean and in other fluids in which dynamic tracers are of interest for a variety of reaction and non-conservative dynamics. Biological rates and physical advection times of interest in the ocean range from hours to days to weeks to months and seasons. A comprehensive review of time scales in the context of this theory could serve both to constrain the theory and guide developments. In addition to the direct extensions discussed in the preceding paragraphs it would be of interest to carry out first studies including new processes such as chaotic trajectories, mixing, swimming and small-scale encounter dynamics. The formulation of more general initial-value problems in the s-domain should be guided not only by direct biological considerations but also by the mathematical structure of the theory of characteristics.

This research was stimulated by several interesting, important and enjoyable scientific discussions with Professor Brian J. Rothschild. I thank Professor A. Denny Kirwan Jr, Professor Eileen E. Hofmann, Dr Patrick J. Haley Jr and Dr Dennis J. McGillicuddy for helpful scientific and mathematical comments. I am grateful to Mr Wayne G. Leslie for his essential contribution to this study by the performance of sensitivity analyses and the preparation of figures. It is a pleasure to thank Dr Nadia Pinardi for the hospitality of Istituto per lo studio delle Metodologie Geofisiche Ambientali (CNR-IMGA) during a sabbatical visit. The preparation of the manuscript by Ms Marsha A. Glass and Mrs Renate D'Arcangelo is very much appreciated. This research was supported in part by the Office of Naval Research under grant N00014–95–1-0371 to Harvard University.

References

Barber, R. T. & Smith, R. L. 1981 Coastal and estuarine fronts. In *Analysis of marine ecosystems* (ed. A. R. Longhurst). New York: Academic.

Batchelor, G. K. 1967 *An introduction to fluid dynamics*. Cambridge University Press.

Bergeron, T. 1928 Über die dreidimensionale verknüpfende Wetteranalyse I. *Geofis. Pub.* **5**, 1–111.

Bowen, A. J., Griffin, D. A., Hazen, D. G., Matheson, S. A. & Thompson, K. R. 1995 Ship-board nowcasting of shelf circulation. *Cont. Shelf Res.* **15**, 115–128.

Courant, R. & Hilbert, D. 1989 Methods of mathematical physics. In *Partial differential equations*, vol. II, p. 830. New York: Wiley Interscience.

Denman, K. L. 1992 Scale determining biological/physical interactions in oceanic food webs. In *Aquatic ecology; scale, pattern and process* (ed. P. S. Giller, A. G. Hildrew & D. G. Raffaelli). Oxford: Blackwell.

Denmam, K. L. & Powell, T. M. 1984 Effects of physical processes on planktonic ecosystems in the coastal ocean. *Oceanogr. Mar. Biol. A. Rev.* **22**, 125–168.

Dewar, W. K. & Flierl, G. R. 1985 Particle trajectories and simple models of transport in coherent vortices. *Dyn. Atmos. Oceans* **9**, 215–252.

Dickey, T. D. 1990 Physical-optical-biological scales relevant to recruitment in large marine ecosystems. In *Large marine ecosystems: patterns, processes, and yields* (ed. K. Sherman, L. M. Alexander & B. D. Gold), publ. no. 90–30s, pp. 82–98. Washington, DC: AAAS.

Flierl, G. R. 1981 Particle motions in large amplitude wave fields. *Geophys. Astrophys. Fluid Dyn.* **18**, 39–74.

Franks, P. J. S., Wroblewski, J. S. & Flierl, G. R. 1986 Prediction of phytoplankton growth in response to the frictional decay of a warm-core ring. *J. Geophys. Res.* **91**, 7603–7610.

Freedman, H. I. 1980 *Deterministic models in population ecology*, p. 254. New York and Basel: Marcel Dekker.

Hinze, J. O. 1975 *Turbulence*, pp. 790. New York: McGraw-Hill.

Horne, J. K. & Schneider, D. C. 1994 Analysis of scale-dependent processes with dimensionless ratios. *OIKOS* **70**, 201–211.

Hoskins, B. J. 1982 The mathematical theory of frontogenesis. *Ann. Rev. Fluid Mech.* **14**, 131–151.

Kirwan Jr, A. D. 1988 Notes on the cluster method for interpretating relative motions. *J. Geophys. Res.* **93**, 9337–9339.

Kirwan Jr, A. D., Lewis, J. K., Indest, A. W., Reinersman, P. & Quintero, I. 1988 Observed and simulated properties of loop current rings. *J. Geophys. Res.* **93**, 1189–1198.

Kirwan Jr, A. D., Indest, A. W., Liu, J. & Clark, N. 1990 Ring evolution in general circulation models from path analysis, *J. Geophys. Res.* **95**, 18 057–18 073.

Kirwan Jr, A. D., Lipphardt Jr, B. L. & Liu, J. 1992 Negative potential vorticity lenses. *Int. J. Eng. Sci.* **30**, 1361–1378.

Kirwan Jr, A. D., Lipphardt Jr, B. L. & Gregory, K. L. 1994 Nonlinear ocean dynamics. In *The oceans: physical-chemical dynamics and human impact* (ed. S. K. Majumdar, E. W. Miller, G. S. Forbes, R. F. Schmalz & A. A. Panah), pp. 40–55. Easton, PA: The Pennsylvania Academy of Science.

Klein, P. & Steele, J. H. 1985 Some physical factors affecting ecosystems. *J. Mar. Res.* **43**, 337–350.

Lamb, H. 1932 *Hydrodynamics*. Cambridge University Press.

Lynch, D. R., Ip, J. T. C., Naimie, C. E. & Werner, F. E. 1995 Convergence studies of tidally-rectified circulation on Georges Bank. In *Quantitative skill assessment for coastal ocean models* (ed. D. R. Lynch & A. M. Davies), Coastal and Estuarine Studies, Am. Geophys. Union **47**, pp. 153–174.

McGillicuddy, D. J., Robinson, A. R. & McCarthy, J. J. 1995 Coupled physical and biological modelling of the spring bloom in the North Atlantic. II. Three-dimensional bloom and post-bloom processes. *Deep Sea Res. I* **42**, 1359–1398.

Murray, J. D. 1993 *Mathematical biology*, p. 767. Berlin: Springer.

Nihoul, J. C. J. & Djenidi, S. 1991 Hierarchy and scales in marine ecohydrodynamics. *Earth-Sci. Rev.* **31**, 255–277.

O'Brien, J. J. & Wroblewski, J. S. 1973 On advection in phytoplankton models. *J. Theor. Biol.* **38**, 197–202.

Okubo, A. 1980 *Diffusion and ecological problems: mathematical models*, p. 254. New York: Springer.

Olson, D. B. & Backus, R. H. 1995 The concentrating of organisms at fronts: a cold-water fish and a warm-core Gulf Stream ring. *J. Mar. Res.* **43**, 113–137.

Ottino, J. M. 1989 *The kinematics of mixing: stretching, chaos and transport*. Cambridge University Press.

Ottino, J. M. 1990 Mixing, chaotic advection and turbulence. *A. Rev. Fluid Mech.* **22**, 207–253.

Petterson, S. 1935 Contribution to the theory of frontogenesis. *Geofis. Pub.* **11**, 1–27.

Platt, T., Denman, K. L. & Jascy, A. D. 1977 Modeling the productivity of phytoplankton. In *Marine modeling, The Sea* (ed. E. D. Goldberg, I. N. McCave, J. J. O'Brien & J. H. Steele), vol. 6, pp. 807–856. New York: Wiley.

Platt, T. & Denman, K. L. 1975 A general equation for the mesoscale distribution of phytoplankton in the sea. *Mem. Soc. Sci. Liege* **7**, 31–42.

Pond, S. & Pickard, G. L. 1978 *Introductory dynamical oceanography*, p. 241. Oxford: Pergamon.

Ring Group, The 1981 Gulf Stream cold-core rings: their physics, chemistry, and biology. *Science* **212**, 1091–1100.

Sanderson, B. G. 1995 Structure of an eddy measured with drifters. *J. Geophys. Res.* **100**, 6761–6776.

Saucier, W. J. 1953 Horizontal deformation in atmospheric motion. *Trans. Am. Geophys. Union* **34**, 709–719.

Simpson, J. H. & James, I. D. 1986 Coastal and estuarine fronts. In *Baroclinic processes on continental shelves* (ed. C. N. K. Mooers), pp. 63–93. Washington, DC: Am. Geophys. Union.

Steele, J. H. 1988 Scale selection for biodynamic theories. In *Toward a theory on biological physical interactions in the world ocean* (ed. B. J. Rothschild), pp. 513–526. Dordrecht: Kluwer.

Stewart, H. J. 1945 Kinematics and dynamics of fluid flow. In *Handbook of meteorology* (ed. F. A. Berry Jr, E. Bollay & N. R. Beers), pp. 412–419. New York: McGraw-Hill.

Stone, P. H. 1966 Frontogenesis by horizontal wind deformation fields. *J. Atmos. Sci.* **23**, 455–465.

Williams, R. T. 1967 Atmospheric frontogenesis: a numerical experiment. *J. Atmos. Sci.* **24**, 627–641.

Wroblewski, J. S. 1983 The role of modeling in biological oceanography. *Ocean Sci. Engng* **8**, 245–285.

Received 28 October 1996; accepted 9 May 1997